Sensor Modeling and Kalman Filtering Applied to Satellite Attitude Determination

By

Joshua Cemenska

BS (University of Illinois at Urbana-Champaign) 2003

A report submitted in partial satisfaction of the Requirements for the degree of

Masters of Science, Plan II

in

Mechanical Engineering

at the

University of California at Berkeley

Committee in Charge:

Professor David Auslander, Chairman
Professor Fai Ma

Fall 2004

Contents

List of Figures

List of Tables

Symbols

Symbol	Unit	Description
A	[-]	Rotation matrix from body to inertial coordinates
q	[-]	Attitude quaternion
e	[-]	Axis vector about which the quaternion rotates.
q''	[-]	Attitude quaternion, distinct from q
q'	[-]	Attitude quaternion that translates from q to q''
I_{xx}	[kg-m^2]	SNAP moment of inertia about its X-axis
I_{yy}	[kg-m^2]	SNAP moment of inertia about its Y-axis
I_{zz}	[kg-m^2]	SNAP moment of inertia about its Z-axis
L	[m]	Effective focal length
θ_L	[rad]	Angular distance from the Z-axis to a point on the focal plane
d_L	[m]	Linear distance from the Z-axis to a point on the focal plane
x_{RMS}	[rad]	Angular standard deviation of a star centroid in the X-direction
y_{RMS}	[rad]	Angular standard deviation of a star centroid in the Y-direction
σ_p	[rad]	Angular standard deviation of a single photon
N_p	[-]	Total number of photons
n_g	[-]	Number of guide stars on focal plane
σ_{rad}	[rad]	Angular standard deviation of a magnitude 16 star
Δt	[sec]	Sample rate of focal plane guiders
σ_d	[m]	Linear standard deviation of a magnitude 16 star on the FGS
r_L	[m]	Distance from the Z-axis to the 1 σ circle around the true star point
θ_{meas}	[rad]	SIRU measured change in attitude angle
$\dot{\theta}_{meas}$	[rad/sec]	Angular velocity which SIRU integrates
f	[Hz]	frequency
s_e^2	[rad^2]	Variance of SIRU angle white noise
s_v^2	[rad^2]	Variance of SIRU angle random walk
s_u^2	[rad^2]	Variance of SIRU rate random walk
σ_e	[rad]	Standard deviation of SIRU angle white noise
σ_v	[rad/sec$^{1/2}$]	Standard deviation of SIRU angle random walk
σ_u	[rad/sec$^{3/2}$]	Standard deviation of SIRU rate random walk
Φ_e	[rad^2/sec]	Power spectral density of SIRU angle white noise
Φ_v	[rad^2/sec]	Power spectral density of SIRU angle random walk
Φ_u	[rad^2/sec]	Power spectral density of SIRU rate random walk
σ	[rad^2]	Total variance of SIRU integrated angle measurement
Δt_g	[sec]	SIRU sample rate

Symbol	Unit	Description
ω_{meas}	[rad/sec]	SIRU angular velocity measurement vector
ω_{true}	[rad/sec]	True angular velocity vector
θ_{true}	[rad]	True change in attitude angle
b	[rad/sec]	SIRU bias vector
b_0	[rad/sec]	SIRU bias vector at the start of each time step
η_1	[rad/sec]	White noise on SIRU rate measurement
η_2	[rad/sec^2]	White noise on rate of change of SIRU bias vector
δ	[-]	Infinite magnitude impulse
ζ_b	[-]	Gaussian random variable with zero-mean and unit variance.
ζ_θ	[-]	Gaussian random variable with zero-mean and unit variance.
Z	[-]	Random variable with zero-mean and unit variance.
b_{est}	[rad/sec]	Kalman filter estimate of SIRU bias
AWN	[rad/Hz$^{1/2}$]	SIRU angle white noise specification
ARW	[rad/sec$^{1/2}$]	SIRU angle random walk noise specification
RRW	[rad/sec$^{3/2}$]	SIRU rate random walk noise specification
J	[-]	A loss function used in attitude determination
J'	[-]	A loss function used in attitude determination
w_k	[-]	Weight assigned to the k^{th} star vector
$\hat{u}_b^k$	[-]	The k^{th} star vector measurement in body coordinates
$\hat{u}_i^k$	[-]	The k^{th} star vector known in inertial coordinates.
I	[-]	Identity matrix
Θ	[-]	A matrix derived from a quaternion
$\tilde{Q}$	[-]	A matrix derived from a quaternion
Γ	[-]	A matrix used in optimization of batch measurements
K'	[-]	A matrix used in optimization of batch measurements
S'	[-]	A matrix used in optimization of batch measurements
B	[-]	A matrix used in optimization of batch measurements
W	[-]	A matrix used in optimization of batch measurements
V	[-]	A matrix used in optimization of batch measurements
σ_B	[-]	Trace of matrix B
q_{est}	[-]	Combined star sensor estimated quaternion
λ_{max}	[-]	The maximum eigenvector of matrix K'
ω	[rad/s]	Angular velocity
Ω	[-]	Matrix formed from angular velocity
$\dot{\Omega}$	[-]	Time derivative of matrix Ω

Symbol	Unit	Description
$\ddot{\Omega}$	[-]	Time derivative of matrix $\dot{\Omega}$
$\bar{\Omega}$	[-]	Time average of matrix Ω
$\bar{\omega}$	[rad/s]	Time average of angular velocity
x	[-]	State vector
w	[-]	Process noise in state propagation
$\hat{x}$	[-]	Estimated state vector
Q	[-]	A matrix representing gyro noise in the Kalman filter
Q_1	[-]	A submatrix of Q
Q_2	[-]	A submatrix of Q
F	[-]	A matrix used in the Kalman filter
G	[-]	A matrix used in the Kalman filter
P	[-]	The state covariance matrix
Φ	[-]	Transition matrix
$\hat{x}_k\,(-)$	[-]	A-priori estimated state vector at the k^{th} time step
$P_k\,(-)$	[-]	A-priori state covariance matrix at the k^{th} time step
K_k	[-]	Kalman gain matrix at the k^{th} time step
$\hat{x}_k\,(+)$	[-]	A-posteriori estimated state vector at the k^{th} time step
$P_k\,(+)$	[-]	A-posteriori state covariance matrix at the k^{th} time step
N	[-]	A matrix used in the Kalman filter
R	[-]	Matrix representing star sensor noise in the Kalman filter
z	[-]	Star sensor measured quaternion used in Kalman filter
h	[-]	Function relating z to the state vector
v_k	[-]	A vector relating star sensor noise at the k^{th} time step
H	[-]	A matrix relating star sensor measurement to the state estimate
θ_y	[rad]	Yaw
ψ_p	[rad]	Pitch
ϕ_r	[rad]	Roll
$\sigma^2_{\theta_y}$	[rad^2]	Variance of yaw measurement
$\sigma^2_{\psi_p}$	[rad^2]	Variance of pitch measurement
$\phi^2_{\theta_r}$	[rad^2]	Variance of roll measurement
R_y	[-]	Star sensor covariance matrix in terms of yaw, pitch, and roll
R_q	[-]	Intermediate matrix used to compute the star sensor noise matrix
H'	[-]	A matrix relating R_q to R
Q'	[-]	Matrix representing quaternion multiplication
Ξ	[-]	A matrix constructed from the estimated quaternion

Symbol	Unit	Description
$\vec{Z}_{true,i}$	[-]	True body z-axis in reference coordinates
$\vec{Z}_{meas,b}$	[-]	Measured body z-axis in true body coordinates
$\vec{X}_{true,i}$	[-]	True body x-axis in reference coordinates
$\vec{X}_{meas,b}$	[-]	Measured body x-axis in true body coordinates
A_{true}	[-]	True rotation matrix
A_{meas}	[-]	Measured rotation matrix
e_{yp}	[rad]	Yaw/pitch error
e_{roll}	[rad]	Roll error
v_1	[-]	Primary star vector
v_2	[-]	Secondary star vector
γ	[rad]	Angular error of star vector on the FGS
α	[rad]	Theoretic angular error of star sensor measurement
$S_{centroid}$	[m]	Linear position of star centroid point on CCD
S_n	[m]	Linear position of an individual star photon on CCD
S	[m]	Linear position of the true star point on the CCD
u	[m/s]	Linear velocity of the true star point on the CCD

Abbreviation	Description
SNAP	Supernova/Acceleration Probe
FGS	Fine guiding sensors
ADS	Attitude determination system
ACS	Attitude control system
SIRU	Space inertial reference unit
AWN	Angle white noise
ARW	Angle random walk
RRW	Rate random walk

Introduction

The Supernova/Acceleration Probe (SNAP) is a satellite equipped with a telescope that is being designed to study the Dark Energy of the Universe. The mission requires an unusually high pointing accuracy of 0.01 arcseconds while science data is being taken. This requirement is to be satisfied by use of an active Attitude Determination and Control System (ACS). Presented here are the sensor modelling and Kalman filtering portions of the larger ACS study. Together these make up the Attitude Determination System (ADS). The study was conducted with the purpose of evaluating the performance of the satellite design. The sensors are central to the SNAP pointing capability, and various combinations of possible sensors are investigated here to determine which sensors should be flown for the mission.

The satellite is equipped with both star sensors and rate measuring gyroscopes. This assessment was done by using Monte Carlo methods to simulate these sensors. Using only star measurements an optimal satellite orientation estimate is found using the method of least squares, and the particular algorithm invoked is referred to as the *q-method* [11].

The satellite is an extremely complicated structure with several sources of dynamic uncertainty, torque noise and disturbances including external torques. According to Lefferts, Markley, and Shuster the problems associated with the large degree of uncertainty in a satellite dynamic model can be avoided by replacing the dynamic model with angular velocity data [10]. Thus the rate measurements obtained from the gyroscopes are combined with the optimal star sensor-determined attitude by means of an extended Kalman filter. This technique provides better attitude estimation than star sensors alone, and using rate data the attitude can be propagated during periods when star sensors are unavailable.

The satellite's telescope is equipped with fine guidance star sensors that provide very accurate pointing. The fine guiding sensors are only available when the telescope is open; however the mission requires accurate pointing even during times when the telescope is closed. The satellite will include less accurate star sensors that contribute to the attitude determination whether or not the telescope sensor is open. Most of the work presented here that involves the star sensors was originally worked out by Anusheh Nawaz, and it appears in her master's thesis [12]. The extended Kalman filter is employed here to improve the attitude determination while only the less accurate star sensors are available.

This report presents the methods used to model and simulate the sensors and Kalman filter as well as the results obtained through simulation. The benefits and abilities of the Kalman filter are discussed. As part of the full ACS study the satellite dynamics are simulated using extensive programming in C++. The dynamic computer model will not be discussed here. For the purposes of this report it is sufficient to say that the true attitude and rotational velocity of the satellite are obtained from the dynamic C++ model.

Chapter 1

Quantifying Satellite Attitude

To discuss the attitude determination system it is first necessary to understand the vocabulary and mathematics that relate to the satellite environment. The following sections present the relevant coordinate systems and discuss how the satellite orientation can be described either by rotation matrices or attitude quaternions. Satellite pointing will be described in terms of 3 components: yaw, pitch, and roll.

1.1 Coordinate Systems

Two coordinate systems are necessary to specify satellite attitude. The inertial coordinate system is a reference coordinate system in which the desired satellite orientation is specified. Typically this coordinate system is referenced to the Earth or to absolute space, and so it is often called world coordinates. There are an infinite number of choices for this coordinate system, but choices involving either the Sun's or the Earth's rotation axis and the celestial sphere are most common. This study assumes that the reference coordinate system is Cartesian, but otherwise arbitrary, and that the desired satellite orientation is known in the reference coordinates. The terms world coordinates and inertial coordinates will be used interchangeably with the term reference coordinates.

The second relevant coordinate system is the satellite body coordinate system. These coordinates are also Cartesian and specified such that the Z-axis is aligned with the boresight (pointing) axis of the telescope. The X-axis and Y-axis point radially outward from the center of the cylindrical satellite.

Satellite orientation is specified by the relationship between reference and body coordinate systems. There are 3 common notations for describing this relationship: rotation matrices, quaternions, and Euler Angles. Euler Angles are not considered here because they have singularities and complicate the attitude determination process. Rotation matrices are commonly referred to as direction cosine matrices. A rotation matrix is a 3×3 matrix that translates a vector from one coordinate system to the other. It is defined here to provide the translation from inertial to body coordinates as shown in equation 1.1 where A is the rotation matrix, v_i is a vector in inertial reference coordinates and v_b is a vector in body

coordinates. Rotation matrix notation is specified as in equation 1.2. The translation from body to inertial coordinates is given by the inverse of the rotation matrix. Because it is an orthonormal matrix the inverse of the rotation matrix equal to its transpose. Rotation matrices contain redundant information, and all of the information provided by the nine element matrix can be condensed into a 4×1 known as a quaternion. Quaternion notation is shown in equation 1.3. Both rotation matrices and quaternions are employed here. Rotation matrices are used to perform the coordinate transformation by a simple matrix multiplication while quaternions are used to dynamically propagate attitude.

$$Av_b = v_i \tag{1.1}$$

$$A = \begin{bmatrix} A_{11}, A_{12}, A_{13} \\ A_{21}, A_{22}, A_{23} \\ A_{31}, A_{32}, A_{33} \end{bmatrix} \tag{1.2}$$

$$q = [q_1, q_2, q_3, q_4]^T \tag{1.3}$$

1.2 Quaternions

Like a rotation matrix a quaternion specifies a 3-dimensional rotation between coordinate systems. The first 3 components of an attitude quaternion designate an axis vector in the reference coordinate system, $e = [e_1, e_2, e_3]^T$. The 4^{th} component specifies the angle of rotation about this axis that will translate any vector in reference coordinates to a vector in the body coordinate system. The quaternion components are related to the angle of rotation by

$$\begin{aligned} q_1 &= e_1 \sin(\phi/2) \\ q_2 &= e_2 \sin(\phi/2) \\ q_3 &= e_3 \sin(\phi/2) \\ q_4 &= \cos(\phi/2) \end{aligned} \tag{1.4}$$

A quaternion can be translated into a rotation matrix as shown by equation 1.5.

$$\begin{aligned} A_{11} &= q_4^2 + q_1^2 - q_2^2 - q_3^2 \\ A_{12} &= 2q_1q_2 + 2q_3q_4 \\ A_{13} &= 2q_1q_3 - 2q_2q_4 \\ A_{21} &= 2q_1q_2 - 2q_3q_4 \\ A_{22} &= q_4^2 - q_1^2 + q_2^2 - q_3^2 \\ A_{23} &= 2q_2q_3 + 2q_1q_4 \\ A_{31} &= 2q_1q_3 + 2q_2q_4 \\ A_{32} &= 2q_2q_3 - 2q_1q_4 \\ A_{33} &= q_4^2 - q_1^2 - q_2^2 + q_3^2 \end{aligned} \tag{1.5}$$

A rotation matrix can be translated to a quaternion using any of 4 distinct algorithms given by equations 1.6 through 1.9. The algorithms are similar in that 1 quaternion component is determined first and then used to find the other 3. When 1 or more components of

the quaternion are near 0 it is important to choose an algorithm appropriate for numerical accuracy. For example in equation 1.6 the 4^{th} quaternion component is determined first and then used to calculate the other components. Because it appears in the denominator of these calculations when the 4^{th} quaternion component is near 0 the other 3 components are sensitive to numeric error. In this case one of the alternative algorithms should be used.

$$\begin{aligned} q_4 &= 0.5\left(1 + A_{11} + A_{22} + A_{33}\right)^{1/2} \\ q_1 &= \tfrac{1}{4q_4}\left(A_{23} - A_{32}\right) \\ q_2 &= \tfrac{1}{4q_4}\left(A_{31} - A_{13}\right) \\ q_3 &= \tfrac{1}{4q_4}\left(A_{12} - A_{21}\right) \end{aligned} \tag{1.6}$$

$$\begin{aligned} q_3 &= 0.5\left(1 - A_{11} - A_{22} + A_{33}\right)^{1/2} \\ q_4 &= \tfrac{1}{4q_3}\left(A_{12} - A_{21}\right) \\ q_2 &= \tfrac{1}{4q_3}\left(A_{23} + A_{32}\right) \\ q_1 &= \tfrac{1}{4q_3}\left(A_{13} + A_{31}\right) \end{aligned} \tag{1.7}$$

$$\begin{aligned} q_2 &= 0.5\left(1 - A_{11} + A_{22} - A_{33}\right)^{1/2} \\ q_1 &= \tfrac{1}{4q_2}\left(A_{12} + A_{21}\right) \\ q_3 &= \tfrac{1}{4q_2}\left(A_{23} + A_{32}\right) \\ q_4 &= \tfrac{1}{4q_2}\left(A_{31} - A_{13}\right) \end{aligned} \tag{1.8}$$

$$\begin{aligned} q_1 &= 0.5\left(1 + A_{11} - A_{22} - A_{33}\right)^{1/2} \\ q_2 &= \tfrac{1}{4q_1}\left(A_{12} + A_{21}\right) \\ q_3 &= \tfrac{1}{4q_1}\left(A_{13} + A_{31}\right) \\ q_4 &= \tfrac{1}{4q_1}\left(A_{23} - A_{32}\right) \end{aligned} \tag{1.9}$$

Quaternion multiplication can be used to translate from one quaternion to another as shown by equation 1.10 where q' is a quaternion that translates from quaternion q to quaternion q''.

$$q'' = \begin{bmatrix} q'_4 & q'_3 & -q'_2 & q'_1 \\ -q'_3 & q'_4 & q'_1 & q'_2 \\ q'_2 & -q'_1 & q'_4 & q'_3 \\ -q'_1 & -q'_2 & -q'_3 & q'_4 \end{bmatrix} q \tag{1.10}$$

Quaternions are defined to have unit magnitude. When any calculations are made with quaternions it is necessary that each input and output quaternion is normalized by its magnitude.

1.3 Yaw, Pitch, Roll

Satellite pointing error is quantified in terms of 3 components: yaw, pitch, and roll; they are shown in figure 1.1. The Z-axis along the boresight of the cylindrical satellite is used to define the error terms. The absolute angle between the desired orientation of this Z-axis

vector and the actual orientation is denoted by yaw and pitch error. Yaw error is specified to be the component of this angle projected onto the desired satellite X-axis vector in reference coordinates while pitch error is specified to be the component projected onto the desired satellite Y-axis vector in reference coordinates. For the SNAP satellite it is not important to distinguish between yaw and pitch, and the absolute angle error will be denoted by yaw/pitch error. Roll error is the angle between the desired satellite X-axis vector and the actual satellite X-axis vector projected onto the plane of the desired Z-axis vector.

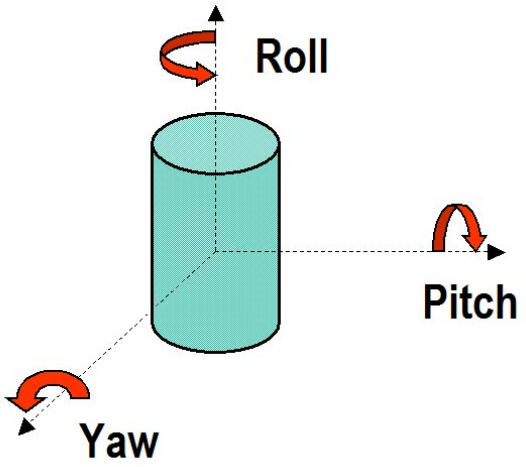

Figure 1.1: Yaw, pitch, and roll with respect to a cylindrical satellite

Because the requirements on SNAP pointing are unusually tight the units for pointing error are reported in arcseconds. One arcsecond is $1/3600^{th}$ degree.

Chapter 2

Satellite Hardware

The SNAP satellite design is a work in progress. Although many of the fine details have not yet been specified there exists sufficient information to conduct the ACS study. The general satellite shape is that of a cylinder with a 2.5 meter diameter and a length of 7.0 meters along its boresight axis. The mass of the satellite is 1600 kg, and the principle moments of inertia are $I_{xx} = 3200$ kg-m, $I_{yy} = 3400$ kg-m, $I_{zz} = 1200$ kg-m where the Z-axis is along the bore-sight [5]. Figure 2.1 shows a view of the exterior of the satellite [7]. The largest feature of the satellite is a 2 meter diameter primary mirror that reflects light through a series of mirrors such that the light shines upon the instrument focal plane. The effective focal length of the telescope mirror assembly is 21.66 m [9]. On the focal plane is an array of light sensitive electronics that have 2 distinct purposes. Most of the electronics will collect the mission science data, but these will not be discussed in this ACS report. Four small electronic patches on the focal plane are designated for attitude determination, and they are referred to as fine guiders. They are charged-coupled devices (CCD's) that collect photons from incoming star rays and detect the point at which each photon is incident. The collected photons are used to determine the direction of a particular star observed by the fine guiders. The focal plane is depicted in figure 2.2 [12]. Considered for SNAP are several sensors. The pointing abilities of various combinations of these sensors are considered in subsequent sections.

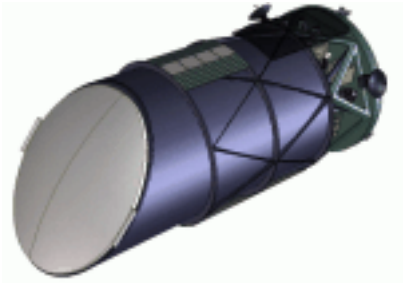

Figure 2.1: The SNAP satellite

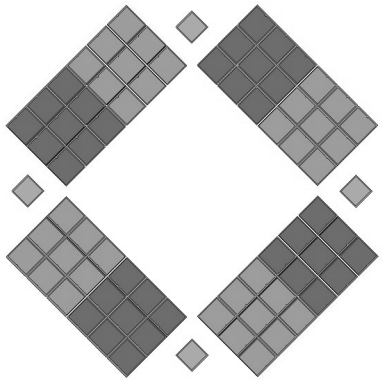

Figure 2.2: The telescope focal plane

2.1 Sensors

1. The focal plane guiders. These sensors are square patches of electronics on the SNAP telescope focal plane. Their placement on the instrument focal plane results in high precision sensors that are of relatively low cost and weight. Each guider is a photon-sensitive charge-coupled device (CCD), which will be custom built and positioned on the SNAP focal plane as shown by the 4 small individual squares in figure 2.2. Each of the 4 CCDs consists of 1000×1000 pixels where each pixel is a square of width 10.5 μm. Each focal plane guider is a square of width 0.0105 m; together they yield a field of view of 200 square arcseconds as specified by [2]. The 4 larger areas on the focal plane are reserved for research measurements. The radius of the focal plane guider CCDs from the center of the focal plane is a design variable and can be measured in either angular or linear distance. Because the primary mirror is an annulus the area illuminated lies between 0.35 degrees and 0.7 degrees from the bore-sight axis [9]. This translates into a radius between 0.128 m and 0.256 m on the focal plane. These sensors have an effective focal length of 21.66 m. The focal plane guider is unavailable during periods when the telescope shutter is closed.

2. The cassegrain guider. This sensor uses the same beam of starlight as the focal plane guider. In contrast to the focal plane guider, it consists of only 1 CCD, located at the center of the beam of starlight. The advantage of this sensor is that it operates even when the telescope shutter is closed.

3. The Ball 602 star trackers. These are commercial sensors with a wide field of view of $8^\circ \times 8^\circ$. Each tracks between 1 and 5 stars per measurement. The effective focal length was modeled to be 0.085 meters. Measurements are taken at 10 Hz. The model for this sensor was derived from [1]. Additional model information was obtained from a phone conversation with Ball Aerospace [15]. Ball 602 star trackers are available whether or not the telescope shutter is closed. They are fully operational up to

an angular velocity of 0.3 degrees per second, and they will operate with reduced performance at up to 1.5 degrees per second.

4. The Northrop Grumman Space Interial Reference Unit (SIRU). The SIRU is an electronics box that contains 4 gyroscopes that measure angular velocity. Only the data from 3 gyroscopes is necessary to determine the 3 components of angular velocity, but the SIRU includes a 4^{th} gyroscope for redundancy. Measurements from the SIRU are available whether or not the telescope shutter is closed. Data from the SIRU is used to replace the dynamic satellite model.

2.2 Sensor Simulation

Figure 2.3 shows the general ACS loop on board the satellite. The sensor system measures the current attitude of the satellite. This signal is compared to the desired value coming from ground control. The difference between target condition and actual condition enters the controller, where the difference is translated into the appropriate command for the actuators. These move the satellite towards the desired position.

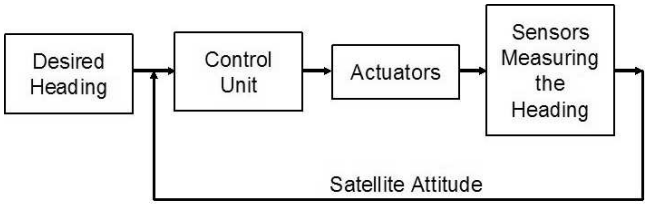

Figure 2.3: The general ACS block diagram

2.2.1 Star Sensor Fundamentals

Star sensors are one of the most accurate means of attitude determination. A star tracker is a star sensor that keeps track of bright stars in its field of view. Star trackers take pictures of the sky, so they are only effective when the satellite is stationary or moving at a slow rate. Maneuvers of the SNAP satellite will be very slow so data from the Ball star trackers will always be available; however the FGS will not be usable during large maneuvers.

The star sensor consists of a lens that refracts the incoming star light rays onto a CCD surface. Figure 2.4 shows the effective focal length model of the optical system [12]. In the figure L is the effective focal length, θ_L is the angular distance between a given point on the focal plane and the satellite Z-axis, and d_L is θ_L translated into a linear distance on the focal plane. The relationship between θ_L, L, and d_L is given by equation 2.1. The small size of the SNAP CCD arrays yields a small angle θ_L, so the relationship between θ_L, L, and d_L is approximately linear.

$$tan(\theta_L) = \frac{d_L}{L} \tag{2.1}$$

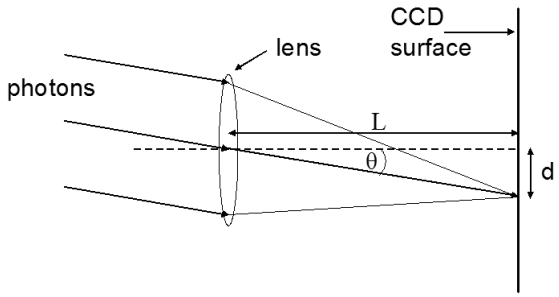

Figure 2.4: The model for the effective focal length

The accuracy of a star tracker is limited by the size of each CCD pixel. The resolution of the tracker is normally the size of 1 pixel; however, greater accuracy can be achieved by centroiding. Centroiding is done by defocusing the incoming star rays such that the distribution of photons from a single ray spreads over several pixels. The centroid of this pattern is used as the star measurement, the resolution of which can be significantly smaller than 1 pixel [13].

Once the position of the star on the CCD is read out the following general steps are taken to determine the attitude [12]:

1. Information about the star, like the brightness, the star pattern and wavelength information, is recorded
2. This information is compared to a imbedded on-board star catalogue, and the star is identified
3. Once the star is identified, its inertial coordinates are known from the star catalogue, and its satellite body coordinates are known from the measurement
4. At least 2 stars are necessary to fully determine the full satellite attitude.

2.2.2 Modeling and Simulation of Star Sensors

Star Sensors are simulated using Monte Carlo methods and statistics. The real star sensor will sense a star over a sample period. During this period the photo-sensitive CCD collects a charge from each incident photon. The total charge on each pixel is read out at the end of a sample period to determine how many photons were incident upon each pixel. Centroiding is performed on the pixel readouts, and this centroid is taken as the star measurement. For a stationary satellite the true star point is stationary, and the individual photons are assumed to be normally distributed about the true point. The accuracy of the measured centroid directly depends on the number of photons collected. If the distance on the CCD

between the true star point and the point intersected by a photon is designated as a random variable then the centroid is an average of a number of random events. Thus the standard deviation of the centroid is related to that of an individual photon, σ_p, by equation 2.2 where N_p is the number of photons and x_{RMS} and y_{RMS} refer to the centroid standard deviation in the X and Y directions respectively.

$$x_{RMS} = y_{RMS} = \frac{\sigma_p}{\sqrt{N_p}} \tag{2.2}$$

The affects of sensor quantum efficiency, pixel size, centroiding and sensor readout noise were investigated in [13]. Secroun, Lampton, and Levi found that the optimum star blur size is 1.5 pixels where each pixel is 10.5 microns (0.1 arcseconds) wide. The optimum number of pixels used for centroiding is 2. Data from that investigation was used to model the sensor noise. Sensor accuracy increases with the number of photons, which increases with star brightness and sample period. Figure 2.5 shows how the centroid standard deviation varies with star brightness and sensor sample rate [13]. Figure 2.6 shows how the probability of having at least 1 star on the focal plane varies with star magnitude, based on the statistical model [13]. Figure 2.6 shows 4 lines for separate suggested designs for the focal plane CCD's. The line which is second from the top is marked by squares and represents the chosen CCD design. It is this line that is relevant to this study.

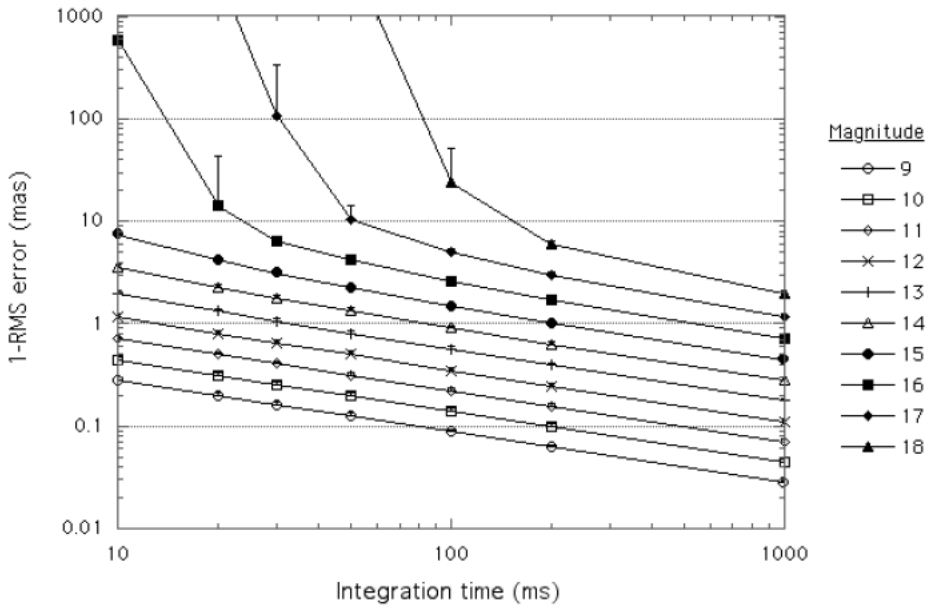

Figure 2.5: The effect of sample rate and star magnitude on the standard deviation of the star centroid on the focal plane

The magnitude of a star measures the brightness. Its scale runs from negative values for very bright objects to positive values as the light source gets dimmer. An increase of 1

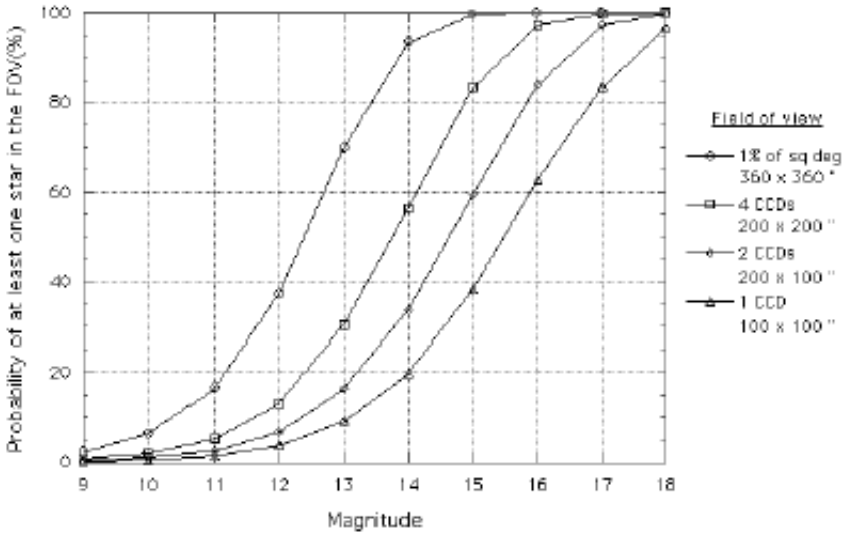

Figure 2.6: The probability of having at least 1 star on the focal plane vs. star magnitude.

unit in magnitude corresponds to a decrease in brightness by a factor of about 2.51. For example a magnitude 5 object is 2.51 times fainter than a magnitude 4 object. The sun has magnitude -26. The brightest star in the Northern sky, Sirius, has magnitude of -1.5 [12].

This ADS study focuses on stars of brightness 16 and a sample rate of 10 Hz. The Ball 602 model and the SIRU standardly output at 10 Hz, so the FGS was set to 10 Hz to coincide with the other sensors. The sample rate governs the frequency of actuation, which could excite structural modes. The stabilization and tracking performance of the satellite controller depends directly on actuation frequency. Because the sensor sample rate affects higher-order components of the satellite the rate that coincides with optimal sensing does not necessarily correspond to the rate for optimal pointing. The sample rate is held at a constant 10 Hz in this attitude determination study. It can be seen in figure 2.6 that the probability of having at least 1 star of brightness 16 or higher on the focal plane is 95%. Because each star is an independent event the probability of n_g stars of brightness 16 or higher is given by equation 2.3. For integration periods longer than 0.03 seconds, the magnitude 16 star noise data of figure 2.5 is equivalent to equation 2.4 for determining angular standard deviation.

$$0.95^{n_g} \tag{2.3}$$

$$\sigma_{rad} = \Delta t^{-1.9642\times10^{-9}} \tag{2.4}$$

where σ_{rad} is the standard deviation of the star centroid in units of radians and Δt is the FGS sample rate in seconds.

The procedure for simulating stars on the FGS was developed by Anushceh Nawaz [12]. The simulation uses a uniform distribution to designate the true position of a star on the FGS. The angular standard deviation of the star centroid was calculated using equation

2.4 for a 10 Hz sample rate and star of brightness 16. The angular standard deviation was translated into an equivalent distance on the CCD, σ_d , using equations 2.5.

$$\begin{aligned} r_L &= L \tan(\theta_L - \sigma_{rad}) \\ \sigma_d &= d_L - r_L \end{aligned} \tag{2.5}$$

where d_L is given by equation 2.1 for a given θ_L, and r_L denotes the distance from the center of the focal plane to the closest point on the 1 standard deviation circle about the true star point, which is located a distance d_L from the center of the focal plane. About the true star position the simulation creates a measured star point using a normal random variable for distance with standard deviation σ_d. The measured star point is distributed circularly about the true star point by designating a second random variable for angle, which has a uniform distribution. This measured star point is then extrapolated into a 3-dimensional vector in satellite body coordinates using the satellite focal length and the star centroid point on the 2-dimensional focal plane. This star vector is used by and attitude determination algorithm to deduce the satellite orientation as described in the following chapter on attitude determination.

Stars observed by the Cassegrain guider are modeled just as for the FGS except that the Cassegrain CCD array is centered on the instrument focal plane.

Stars observed by the Ball 602 star tracker are modeled each with a standard deviation of 1.5 arcseconds on the 602's focal plane.

2.2.3 Gyroscope Simulation

Gyroscopes are instruments commonly used on-board spacecraft to measure angular velocity. The gyroscope model used for SNAP is a hemispherical resonating gyroscope (HRG), 4 of which are included in the space inertial reference unit (SIRU). The HRG model to be used on SNAP is a rate-integrating gyro, which means that it outputs change in angle, θ_{meas}, instead of angular velocity, as shown by equation 2.6. Satellite attitude cannot be obtained from the gyro measurements alone. Because the SIRU outputs a change in angle, an initial orientation is necessary to determine the current orientation. Over time gyroscopes accumulate a bias that must be periodically removed for the gyro measurements to be useful. The Kalman filter, which is described in section 3.2, is used to remove the gyro bias.

$$\theta_{meas} = \int_0^{\Delta t_g} \dot{\theta}_{meas} dt \tag{2.6}$$

Farrenkopf developed an accurate model for rate integrating gyroscopes operating in the rate mode [4]. The mathematical model used here for the gyroscope follows his formulation, which is the form used in the Kalman filter model described by Lefferts, Markley, and Shuster [10].

In the model, noise is divided into 3 independent components. The SIRU noise specifications also describe noise in 3 independent components: rate random walk (RRW), angle

white noise (AWN), and angle random walk (ARW). Rate random walk is modeled as a white noise that is added to the derivative of a rate measurement. The random walk is mathematically the same as Brownian motion. Because the SIRU outputs integrated rate, the RRW appears as double-integrated white noise. Angle random walk is a noise component modeled as white noise added to the rate measurement. Because the SIRU outputs integrated rate this term appears as integrated white noise. Angle white noise is white noise added to the change in angle that is output from the gyroscope. Some work is necessary to correlate these simulation specifications to the Farrenkopf model. The development of equations shown here follows from the detailed description provided in a technical paper for the NASA GOES Project [18]. To first and second order the simulation model can be matched to the the Farrenkopf model by matching linear and quadratic expected values of the measurement and measurement bias, as developed in the remaining portion of this section.

Angle white noise represents the band-limited noise that originates in the high frequency electronic components of a gyroscope. The variance of band-limited noise, s_e^2 , is the square of the standard deviation, σ_e, as shown by equation 2.7 [17]. The term Φ designates the power spectral density function of the random process.

$$s_e^2 = 2\int_{f_1}^{f_2} \Phi_e\left(f\right) df = 2\int_{f_1}^{f_2} \frac{\sigma_e^2}{2\left(f_2 - f_1\right)} df = \sigma_e^2 \tag{2.7}$$

Angle random walk models mid-frequency noise. The variance, s_v^2, is related to the standard deviation, σ_v, as shown by equation 2.8 [17].

$$s_v^2 = 2\int_{f_1}^{f_2} \Phi_v\left(f\right) df = 2\int_{f_1}^{f_2} \frac{\sigma_v^2}{2f^2} df = \sigma_v^2\left(\frac{1}{f_1} - \frac{1}{f_2}\right) \tag{2.8}$$

Rate random walk models low-frequency noise. The variance, s_u^2, is related to the standard deviation, σ_u, as shown by equation 2.9 [17].

$$s_u^2 = 2\int_{f_1}^{f_2} \Phi_u\left(f\right) df = 2\int_{f_1}^{f_2} \frac{\sigma_u^2}{2f^4} df = \frac{\sigma_v^2}{3}\left(\frac{1}{f_1^3} - \frac{1}{f_2^3}\right) \tag{2.9}$$

The variances of AWN, ARW, and RRW add together to give the total gyro noise variance, which is the square of the total standard deviation, as shown by equation 2.10 [17].

$$\sigma = \left(s_e^2 + s_v^2 + s_u^2\right)^{1/2} = \left(\sigma_e^2 + \sigma_v^2\left(\frac{1}{f_1} - \frac{1}{f_2}\right) + \frac{\sigma_u^2}{3}\left(\frac{1}{f_1^3} - \frac{1}{f_2^3}\right)\right)^{1/2} \tag{2.10}$$

The frequency band to consider for the gyroscope noise is from $f_1 = 1/\Delta t_g$ to $f_2 \to \infty$, where Δt_g is the sample rate of the gyro. In this frequency band equation 2.10 becomes equation 2.11.

$$\sigma = \left(\sigma_e^2 + \sigma_v^2 \Delta t_g + \frac{\sigma_u^2}{3}\left(\Delta t_g^3\right)\right)^{1/2} \tag{2.11}$$

The Farrenkopf model for a gyroscope is given by equations 2.12 and 2.13 [10].

$$\omega_{meas} = \dot{\theta}_{meas} = \omega_{true} + b + \eta_1 \tag{2.12}$$

$$\dot{b} = \eta_2 \tag{2.13}$$

where b is the gyro bias vector, $[b_x, b_y, b_z]^T$, and $\dot{\theta}_{meas}$ and ω_{true} are respectively the measured and true rate of change of the satellite orientation about the axis aligned with the gyroscope. Both η_1 and η_2 are zero-mean, white noise processes. Since the processes are zero-mean, the expected value of each is 0, as shown by equation 2.14.

$$E\{\eta_1\} = E\{\eta_2\} = 0 \tag{2.14}$$

It is assumed that η_1 and η_2 are independent at any times, t and t' and satisfy equation 2.15.

$$E\{\eta_1(t)\,\eta_2(t')\} = 0 \tag{2.15}$$

Because η_1 and η_2 are white, each is uncorrelated with itself at any 2 distinct times, t and t', as shown by equations 2.16, where $\delta(\rho)$ represents a unit impulse with infinite magnitude at $\rho = 0$ and magnitude 0 at $\rho \neq 0$.

$$\begin{aligned} E\{\eta_1(t)\,\eta_1(t')\} &= \left(\sigma_v^2 + \tfrac{\sigma_e^2}{\Delta t_g}\right)\delta(t-t') \\ E\{\eta_2(t)\,\eta_2(t')\} &= \sigma_u^2\delta(t-t') \end{aligned} \tag{2.16}$$

In equation 2.16 the $\frac{\sigma_e^2}{\Delta t_g}$ term enters because the rate measurement is modeled as the numerical derivative of the change in angle measurement. The gyro bias can be solved for from equation 2.13. The result is equation 2.17, where b_0 is the value of the bias at the beginning of each time step.

$$b = b_0 + \int_0^{\Delta t_g} \eta_2(t)dt \tag{2.17}$$

The expected value of b is just its value at the beginning of the time step.

$$E\{b\} = b_0 \tag{2.18}$$

The expected value of b^2 can next be found by squaring both sides of equation 2.17 and taking the expectation. Using equations 2.16 and 2.14:

$$\begin{aligned} E\{b^2\} &= E\{b_0^2\} + E\left\{2b_0\textstyle\int_0^{\Delta t_g}\eta_2(t)\,dt\right\} + E\left\{\textstyle\int_0^{\Delta t_g}\eta_2(t)\,dt\int_0^{\Delta t_g}\eta_2(t')\,dt'\right\} \\ &= b_0^2 + \sigma_u^2\textstyle\int_0^{\Delta t_g}\int_0^{\Delta t_g}\delta(t-t')\,dtdt' \\ &= b_0^2 + \sigma_u^2\Delta t_g \end{aligned} \tag{2.19}$$

Equations 2.18 and 2.19 are satisfied by defining the gyroscope bias simulation model by equation 2.20, where ζ_b is a gaussian-distributed random variable with zero-mean and unit variance.

$$b = b_0 + \sigma_u \left(\Delta t_g\right)^{1/2} \zeta_b \tag{2.20}$$

Combining equations 2.12, 2.20, and 2.6 the gyroscope output can be expressed by equation 2.21.

$$\theta_{meas} = \theta_{true} + b_0 \Delta t_g + \int_0^{\Delta t_g} \int_0^t \eta_2 \left(\tau\right) d\tau dt + \int_0^{\Delta t_g} \eta_1 \left(t\right) dt \tag{2.21}$$

The expected values of θ and $b\theta$ are given by equations 2.22 and 2.23, respectively.

$$E\left\{\theta\right\} = \theta_{true} + b_0 \Delta t_g \tag{2.22}$$

$$\begin{aligned} E\left\{b\theta\right\} &= E\left\{\left[b_0 + \int_0^{\Delta t_g} \eta_2 \left(t\right) dt\right]\left[\theta_{true} + b_0 \Delta t_g + \int_0^{\Delta t_g} \int_0^t \eta_2 \left(\tau\right) d\tau dt\right]\right\} \\ &\quad + E\left\{\left[b_0 + \int_0^{\Delta t_g} \eta_2 \left(t\right) dt\right]\left[\int_0^{\Delta t_g} \eta_1 \left(t\right) dt\right]\right\} \\ &= b_0 \left(\theta_{true} + b_0 \Delta t_g\right) + E\left\{\int_0^{\Delta t_g} \eta_2 \left(t'\right) dt' \int_0^{\Delta t_g} \int_0^t \eta_2 \left(\tau\right) d\tau dt\right\} \\ &= b_0 \left(\theta_{true} + b_0 \Delta t_g\right) + \sigma_u^2 \int_0^{\Delta t_g} \int_0^{\Delta t_g} \int_0^t \delta\left(t' - \tau\right) d\tau dt' dt \\ &= b_0 \left(\theta_{true} + b_0 \Delta t_g\right) + \sigma_u^2 \int_0^{\Delta t_g} t dt = b_0 \left(\theta_{true} + b_0 \Delta t_g\right) + \frac{\sigma_u^2 (\Delta t_g)^2}{2} \end{aligned} \tag{2.23}$$

Equations 2.23 and 2.22 are satisfied by modeling the measured change in angle by equation 2.24.

$$\begin{aligned} \theta_{meas} &= \theta_{true} + b_0 \Delta t_g + \tfrac{1}{2} \sigma_u \Delta t^{3/2} \zeta_b + Z \\ &= \theta_{true} + \left(b_0 + b\right) \tfrac{\Delta t_g}{2} + Z \end{aligned} \tag{2.24}$$

where Z is a zero-mean random variable that is uncorrelated with ζ_b. The random variable Z will be used to match the model to the expected value of θ_{meas}^2. The expected value of θ_{meas}^2 can be found by squaring both sides of equation 2.21, as shown in equation 2.25.

$$\begin{aligned} E\left\{\theta_{meas}^2\right\} &= \left(\theta_{true} + b_0 \Delta t_g\right)^2 + E\left\{\int_0^{\Delta t_g} \int_0^t \eta_2 \left(\tau\right) d\tau dt \int_0^{\Delta t_g} \int_0^{t'} \eta_2 \left(\tau'\right) d\tau' dt'\right\} \\ &\quad + E\left\{\int_0^{\Delta t_g} \eta_1 \left(t\right) dt \int_0^{\Delta t_g} \eta_1 \left(t'\right) dt'\right\} \\ &= \left(\theta_{true} + b_0 \Delta t_g\right)^2 + \sigma_u^2 \int_0^{\Delta t_g} \int_0^{\Delta t_g} \int_0^t \int_0^{t'} \delta\left(\tau - \tau'\right) d\tau' d\tau dt' dt \\ &\quad + \left(\sigma_v^2 + \tfrac{\sigma_e^2}{\Delta t_g}\right) \int_0^{\Delta t_g} \int_0^{\Delta t_g} \delta\left(t - t'\right) dt dt' \\ &= \left(\theta_{true} + b_0 \Delta t_g\right)^2 + \sigma_u^2 \int_0^{\Delta t_g} \int_0^{\Delta t_g} \min\left(t, t'\right) dt' dt + \left(\sigma_v^2 + \tfrac{\sigma_e^2}{\Delta t_g}\right) \Delta t_g \end{aligned} \tag{2.25}$$

The remaining integral can be split into parts where $t' < t$ and $t' > t$, as shown in equation 2.26.

$$\begin{aligned}\sigma_u^2 \int_0^{\Delta t_g} \int_0^{\Delta t_g} \min(t,t')\, dt' dt &= \int_0^{\Delta t_g} \left[\int_0^t t' dt' + \int_0^{\Delta t_g} t dt'\right] dt \\ &= \int_0^{\Delta t_g} \left[\tfrac{t^2}{2} + t(\Delta t_g - t)\right] dt \\ &= \Delta t_g \int_0^{\Delta t_g} t dt - \tfrac{1}{2}\int_0^{\Delta t_g} t^2 dt \\ &= \tfrac{\Delta t_g^3}{3}\end{aligned} \tag{2.26}$$

Thus

$$E\left\{\theta_{meas}^2\right\} = \left(\theta_{true} + b_0 \Delta t_g\right)^2 + \sigma_u^2 \frac{\Delta t_g}{3} + \left(\sigma_v^2 + \frac{\sigma_e^2}{\Delta t_g}\right) \Delta t_g \tag{2.27}$$

The expectation of the simulation model θ_{meas}^2 is

$$E\left\{\theta_{meas}^2\right\} = \left(\theta_{true} + b_0 \Delta t_g\right)^2 + \sigma_u^2 \frac{\left(\Delta t_g\right)^3}{4} + E\left\{Z^2\right\} \tag{2.28}$$

Equating equations 2.27 and 2.28 yields

$$E\left\{Z^2\right\} = \left(\sigma_v^2 + \frac{\sigma_e^2}{\Delta t_g}\right) \Delta t_g + \sigma_u^2 \frac{\left(\Delta t_g\right)^3}{12} \tag{2.29}$$

which is satisfied by modeling Z by

$$Z = \left(\sigma_e^2 + \sigma_v^2 \Delta t_g + \sigma_u^2 \frac{\left(\Delta t_g\right)^3}{12}\right)^{1/2} \zeta_\theta \tag{2.30}$$

The term ζ_θ is a gaussian-distributed random variable with zero-mean and unit variance. It is uncorrelated with ζ_b.

The final simulation model relies on 2 equations: 2.20 and 2.31.

$$\theta_{meas} = \theta_{true} + \left(b_0 + b\right) \frac{\Delta t_g}{2} + \left(\sigma_e^2 + \sigma_v^2 \Delta t_g + \sigma_u^2 \frac{\left(\Delta t_g\right)^3}{12}\right)^{1/2} \zeta_\theta \tag{2.31}$$

The SIRU angular velocity measurement, ω_{meas}, is then created numerically by equation 2.32.

$$\omega_{meas} = \frac{\theta_{meas}}{\Delta t_g} - b_{est} \tag{2.32}$$

where b_{est} is the gyro bias estimated by the Kalman filter. The SIRU specification are related to the various simulated standard deviations by

$$\begin{aligned} \sigma_e &= AWN[rad]\left(\frac{\Delta t_g}{2}\right)^{1/2} \\ \sigma_v &= ARW[rad/s^{1/2}] \\ \sigma_u &= RRW[rad/s^{3/2}] \end{aligned} \tag{2.33}$$

According to Ball Aerospace Inc. the SIRU specifications are: AWN = 0.0035 arcsec/$\text{Hz}^{1/2}$, RRW = 9.495e-5 arcsec/$\text{s}^{3/2}$ [16]. According to Northrop Grumman: ARW = 0.0001 deg/$\text{hr}^{1/2}$ [8]. For use in the Kalman filter it is important that the units of σ_e be in rad, the units of σ_v be in rad/$\text{s}^{1/2}$, and the units of σ_u be in rad/$\text{s}^{3/2}$.

Chapter 3

Attitude Determination

Attitude determination is necessary to perform accurate telescope measurements, to maneuver the satellite, and to communicate with ground stations on Earth. Furthermore, the telescope must be kept from pointing at the Sun, and the solar panel must be kept oriented toward the Sun to power the satellite.

SNAP will have several sensors that are capable of determining attitude independently. This chapter explains how the instruments individually determine attitude and how the sensor measurements can be combined to yield an attitude estimate that is more accurate than that provided by any individual sensor.

The multiple star sensors determine attitude using a process referred to as the *q-method* as described in [11]. To obtain the full 3-axis attitude at least 2 star vectors must be known in inertial coordinates and measured in satellite body coordinates. The *q-method* minimizes a loss function involving 2 or more weighted star vector measurements. This minimization provides an optimal solution for a given set of star observations.

The SIRU uses measurements of angular velocity to propagate the estimated attitude forward in time from an initial estimate.

The Kalman filter uses the SIRU rate measurement in place of a dynamic model of the satellite to propagate forward in time the estimated attitude and its noise statistics. The propagated attitude is then weighted and blended with the next attitude measurement to provide an optimal attitude estimate based on both SIRU and star sensor measurements.

3.1 Three Axis Attitude Determination: the q-Method

The *q-method* of attitude determination provides an optimal estimate based on multiple star observations. The estimate is optimal because it minimizes the loss function, $J(A^{-1})$ in equation 3.1, where J is the loss, n_s is the number of star observations, A^{-1} is the inverse of the rotation matrix as defined by equation 1.1, w_k is a weight assigned to the k^{th} measurement, $\hat{u}_b^k$ is the k^{th} star vector measurement in body coordinates, and $\hat{u}_i^k$ is the k^{th}

star vector known in inertial coordinates.

$$J(A) = \sum_{k=1}^{n_s} w_k \left| \hat{u}_b^k - A\hat{u}_i^k \right|^2 \tag{3.1}$$

The following procedure for minimizing the loss function is taken from a technical article by Lerner [11]. The loss function can be written as

$$J(A) = -2\sum_{k=1}^{n_s} W_k A^{-1} V_k + \text{constant terms} \tag{3.2}$$

with

$$\begin{aligned} W_k &= \sqrt{w_k}\hat{u}_b^k \\ V_k &= \sqrt{w_k}\hat{u}_i^k \end{aligned} \tag{3.3}$$

Minimizing $J(A^{-1})$ is equivalent to maximizing a second loss function, $J'(A^{-1})$, which is maximum when

$$J'(A^{-1}) = \sum_{k=1}^{n_s} W_k A^{-1} V_k \equiv tr\left(W^T A^{-1} V\right) \tag{3.4}$$

where W and V are the $3 \times n_s$ matrices

$$\begin{aligned} W &\equiv [W_1 |\, W_2 | \cdots |\, W_n] \\ V &\equiv [V_1 |\, V_2 | \cdots |\, V_n] \end{aligned} \tag{3.5}$$

Next the rotation matrix inverse is parameterized in terms of its quaternion by

$$A^{-1}(q) = \left(q_4^2 - q_1^2 - q_2^2 - q_3^2\right) I + 2\Theta - 2q_4\tilde{Q} \tag{3.6}$$

where I is a 3×3 identity matrix, q_k denotes the k^{th} component of the quaternion for the inverse of the rotation matrix, and Θ and $\tilde{Q}$ are defined as

$$\begin{aligned} \Theta &= \begin{bmatrix} q_1q_1 & q_1q_2 & q_1q_3 \\ q_2q_1 & q_2q_2 & q_2q_3 \\ q_3q_1 & q_3q_2 & q_3q_3 \end{bmatrix} \\ \tilde{Q} &= \begin{bmatrix} 0 & -q_3 & q_2 \\ q_3 & 0 & -q_1 \\ -q_2 & q_1 & 0 \end{bmatrix} \end{aligned} \tag{3.7}$$

As shown by Keat [6] after considerable matrix algebra the second loss function can be expressed by

$$J'(q) = q^T K' q \tag{3.8}$$

where

$$K' = \begin{pmatrix} S' - I\sigma_B & \Gamma \\ \Gamma^T & \sigma_B \end{pmatrix} \tag{3.9}$$

$$B \equiv WV^T \tag{3.10}$$

$$S' \equiv B^T + B \tag{3.11}$$

$$\Gamma \equiv (B_{23} - B_{32}, B_{31} - B_{13}, B_{12} - B_{21})^T \tag{3.12}$$

$$\sigma_B \equiv tr\,(B) \tag{3.13}$$

Using Lagrange multipliers it can be shown that the maximum of J' is achieved when the estimated quaternion, q_{est} is equal to the maximum eigenvector, λ_{max}, of the matrix K'.

$$q_{est} = \lambda_{\max}\,(K') \tag{3.14}$$

The optimum quaternion estimate can then be converted back to find the inverse of the rotation matrix, which can be transposed to find the optimum rotation matrix estimate. This provides the optimum attitude estimate based on star observations from the star sensors. The estimate can be improved using the SIRU and Kalman filter.

3.1.1 Weighting of Observations

Because there are multiple types of sensors on the SNAP satellite, the weighting of a star vector measurement from each type of sensor receives a distinct weight in equation 3.1. The above loss function procedure yields the optimum attitude estimate for a given set of weights without specifying how the weights are determined.

The weighting scheme chosen for this simulation follows that for 2 independent measurements for a simple linear system. Because the SNAP ADS is much more complex the weighting algorithm is not proposed to be optimal, but it does assign weights in a systematic manner that effectively reduces attitude estimation error.

Consider a scalar quantity, x the value of which is desired. There are 2 independent sources of measurement of x. They are y and z, and their variances are known to be σ_y^2 and σ_z^2. An optimal weight, $\hat{w}$ is sought such that

$$x = (1 - \hat{w})y + \hat{w}z \tag{3.15}$$

Notice that the weight for y, $(1 - \hat{w})$, and for z, $\hat{w}$, add to 1. An optimal weight minimizes the variance of x, σ_x^2.

$$\begin{aligned} \sigma_x^2 &= E\left\{(x - E\,(x))^2\right\} \\ &= \vdots \\ &= (1 - \hat{w})^2\,\sigma_y^2 + \hat{w}^2\sigma_z^2 \end{aligned} \tag{3.16}$$

To minimize σ_x^2 with respect to $\hat{w}$

$$\frac{\partial \sigma_x^2}{\partial \hat{w}} = \frac{\partial}{\partial \hat{w}} \left((1-\hat{w})^2 \sigma_y^2 + \hat{w} \sigma_z^2 \right) = 0 \tag{3.17}$$

for which the solution is

$$\hat{w} = \frac{\sigma_y^2}{\sigma_y^2 + \sigma_z^2} \tag{3.18}$$

This result is applied to the star vectors measured by the SNAP FGS and the Ball 602 star trackers, where σ_y^2 is replaced by the angular variance of the star measurement on the FGS and σ_z^2 is replaced by the angular variance of the star measurement on the Ball 602 star tracker.

3.1.2 Attitude Propagation using a Gyroscope

By measuring angular velocities the gyroscope can be used as a second source of estimated attitude. Spence and Markley have presented a method of propagating an attitude quaternion in time using rate measurements [14]. The equations reported in this section follow his procedure. Attitude quaternion dynamics are expressed by the following ordinary differential equation:

$$\frac{d}{dt} q(t) = \frac{1}{2} \Omega(w(t)) q(t) \tag{3.19}$$

where ω is the 3×1 angular velocity vector in body coordinates, and Ω is a 3×3 matrix given by

$$\Omega(\omega) = \begin{bmatrix} 0 & \omega_z & -\omega_y & \omega_x \\ -\omega_z & 0 & \omega_x & \omega_y \\ \omega_y & -\omega_x & 0 & \omega_z \\ -\omega_x & -\omega_y & -\omega_z & 0 \end{bmatrix} \tag{3.20}$$

Assuming a constant sample rate and that the angular velocity in body coordinates is constant over the sample period, a closed form solution is shown in equation 3.21.

$$q(t_{k+1}) = e^{\frac{1}{2}\Omega_k \Delta t_g} q(t_k) \tag{3.21}$$

where k represents the k^{th} sample and Δt_g is the SIRU sample rate. For reasonably fast sample periods the assumption of constant angular velocity is good. Equation 3.21 is expanded into a Taylor series for simulation.

$$q(t_{k+1}) = q(t_k) + \frac{dq}{dt}\Delta t_g + \frac{1}{2}\frac{d^2 q}{dt^2}\Delta t_g^2 + \cdots \tag{3.22}$$

By repeated use of equation 3.19, equation 3.22 can be expressed as

$$\begin{aligned} q(t_{k+1}) = &\left[I + \tfrac{1}{2}\Delta t_g \Omega_k + \tfrac{1}{4}\tfrac{\Delta t_g^2 \Omega_k^2}{2!} + \tfrac{1}{8}\tfrac{\Delta t_g^3 \Omega_k^3}{3!} + \cdots \right] q(t_k) + \tfrac{1}{4}\Delta t_g^2 \dot{\Omega}_k q(t_k) \\ &+ \left[\tfrac{1}{12}\dot{\Omega}_k \Omega_k + \tfrac{1}{24}\Omega_k \dot{\Omega}_k \right] \Delta t_g^3 q(t_k) + \tfrac{1}{12}\Delta t_g^3 \ddot{\Omega}_k q(t_k) + \cdots \end{aligned} \tag{3.23}$$

Because the angular velocities are not constant over the sampler period the average angular velocity is obtained from the SIRU measurements such that

$$\bar{\Omega} \equiv \frac{1}{\Delta t_g}\int_{t_k}^{t_{k+1}} \Omega\left(t\right)dt = \Omega_k + \frac{1}{2}\dot{\Omega}_k\Delta t_g + \frac{1}{6}\ddot{\Omega}_k\Delta t_g^2 \tag{3.24}$$

To make use of the average angular velocities obtained from the SIRU, equation 3.23 is rearranged into equation 3.25.

$$\begin{aligned} q\left(t_{k+1}\right) = &\left[I + \tfrac{1}{2}\Delta t_g\bar{\Omega} + \tfrac{1}{4}\tfrac{\Delta t_g^2\bar{\Omega}^2}{2!} + \tfrac{1}{8}\tfrac{\Delta t_g^3\bar{\Omega}^3}{3!} + \cdots\right] q\left(t_k\right) \\ &+\tfrac{1}{48}\left[\dot{\Omega}_k\Omega_k - \Omega_k\dot{\Omega}_k\right]\Delta t_g^3 q\left(t_k\right) + \cdots \end{aligned} \tag{3.25}$$

The second set of bracketed terms in equation 3.25 is small and neglected for simulation. Simplified and truncated, equation 3.26 is used with the gyroscope angular velocity measurement in order to propagate the satellite attitude in time.

$$q\left(t_{k+1}\right) = \left[I + \frac{1}{2}\Delta t_g\bar{\Omega} + \frac{1}{4}\frac{\Delta t_g^2\bar{\Omega}^2}{2!} + \frac{1}{8}\frac{\Delta t_g^3\bar{\Omega}^3}{3!}\right] q\left(t_k\right) \tag{3.26}$$

Given the quaternion at to distinct moments in time separated by Δt_g the approximate average angular velocity, $\bar{\omega}$ can be calculated by

$$\begin{bmatrix} \bar{\omega}_x \\ \bar{\omega}_y \\ \bar{\omega}_z \end{bmatrix} = \frac{2}{\Delta t_g}\begin{bmatrix} q_4\left(t_k\right) & -q_3\left(t_k\right) & q_2\left(t_k\right) \\ q_3\left(t_k\right) & q_4\left(t_k\right) & -q_1\left(t_k\right) \\ -q_2\left(t_k\right) & q_1\left(t_k\right) & q_4\left(t_k\right) \end{bmatrix}^{-1}\begin{bmatrix} q_1\left(t_k\right) - q_1\left(t_{k+1}\right) \\ q_2\left(t_k\right) - q_2\left(t_{k+1}\right) \\ q_3\left(t_k\right) - q_3\left(t_{k+1}\right) \end{bmatrix} \tag{3.27}$$

3.2 The Extended Kalman Filter

The Kalman filter is a means of obtaining an optimal estimate of satellite attitude given a dynamic model, sensor measurements, and noise characteristics of the sensors and actuators. Lefferts, Markley, and Shuster provide an overview of Kalman filter theory applied to spacecraft attitude determination [10]. Their report compiles successful methods of Kalman filtering used in that area. The algorithm they present differs from standard Kalman filter theory in that the satellite dynamic model is replaced with the angular velocity measurements from a gyroscope. This avoids dynamic model accuracy problems that stem from externally applied torques and the complexity of spacecraft equipment.

3.2.1 Kalman Filter Theory

As a 3-dimensional object rotating in space, a satellite dynamic equations of motion are inherently nonlinear; the Kalman filter applied to this nonlinear system is an extended Kalman filter. A general state equation is written

$$\frac{d}{dt}x\left(t\right) = f\left(x\left(t\right), t\right) + g\left(x\left(t\right), t\right)w\left(t\right) \tag{3.28}$$

where $x(t)$ is the state vector as a function of time and $w(t)$ is process noise. The functions f and g are system dependent. The noise, w, is assumed to be zero-mean and gaussian-distributed with variance described by equation 3.30.

$$E\left\{w\left(t\right)\right\} = 0 \tag{3.29}$$

$$E\left\{w\left(t\right)w^{T}\left(t\right)\right\} = Q\left(t\right)\delta\left(t-t'\right) \tag{3.30}$$

where $\delta(\rho)$ represents a unit impulse with infinite magnitude at $\rho = 0$ and magnitude 0 at $\rho \neq 0$. The matrix Q is system dependent. The initial values of mean and covariance of the state are denoted as

$$E\left\{x\left(t_0\right)\right\} \equiv \hat{x}\left(t_0\right) = x_0 \tag{3.31}$$

$$E\left\{\left[x\left(t_0\right)-x_0\right]\left[x\left(t_0\right)-x_0\right]^{T}\right\} \equiv P\left(t_0\right) = P_0 \tag{3.32}$$

where $\hat{x}$ denotes the estimate of the state. It is assumed that the initial mean of the state is known and set equal to the initial state estimate. It is also assumed that the initial state covariance is known. Based on equation 3.28 the minimum variance estimate of the state at time t in the future is given by a conditional expectation

$$\hat{x}\left(t\right) = E\left\{x\left(t\right)\middle|\, x_0\right\} \tag{3.33}$$

Because $w(t)$ is white, the expected dynamic equation becomes

$$\frac{d}{dt}\hat{x}\left(t\right) = f\left(\hat{x}\left(t\right), t\right) \tag{3.34}$$

Integrating equation 3.34 gives

$$\hat{x}\left(t\right) = \phi\left(t, \hat{x}\left(t_0\right), t_0\right) \tag{3.35}$$

The state error vector is defined as

$$\Delta x\left(t\right) = x\left(t\right) - \hat{x}\left(t\right) \tag{3.36}$$

The state covariance matrix can then be defined by

$$P\left(t\right) = E\left\{\Delta x\left(t\right)\Delta x^{T}\left(t\right)\right\} \tag{3.37}$$

By neglecting terms that are higher than first order, the dynamic equation for the state error vector can be written as

$$\frac{d}{dt}\Delta x\left(t\right) = \frac{\partial}{\partial x}f\left(x,t\right)\Big|_{\hat{x}(t)}\Delta x\left(t\right) + g\left(\hat{x}\left(t\right), t\right) \tag{3.38}$$

To simplify notation F and G are defined:

$$\begin{aligned} F\left(t\right) &\equiv \tfrac{\partial}{\partial x}f\left(x,t\right)\big|_{\hat{x}(t)} \\ G\left(t\right) &\equiv g\left(\hat{x}\left(t\right), t\right) \end{aligned} \tag{3.39}$$

The linearization that has been applied in equation 3.38 approximates the nonlinear system with a linear system to which the linear Kalman filter equations can be applied. Integrating equation 3.38 gives

$$\Delta x\left(t\right)=\Phi\left(t,t_0\right)\Delta t_0+\int_{t_0}^{t}\Phi\left(t,t'\right)G\left(t'\right)w\left(t'\right)dt' \tag{3.40}$$

where Φ is a transition matrix that satisfies

$$\begin{aligned}\tfrac{\partial}{\partial t}\Phi\left(t,t_0\right)&=F\left(t\right)\Phi\left(t,t_0\right)\\ \Phi\left(t_0,t_0\right)&=I\end{aligned} \tag{3.41}$$

The propagation of the covariance matrix satisfies the following Riccati equation:

$$\frac{d}{dt}P\left(t\right)=F\left(t\right)P\left(t\right)+P\left(t\right)F^T\left(t\right)+G\left(t\right)Q\left(t\right)G^T\left(t\right) \tag{3.42}$$

Integrating the Riccati equation gives

$$P\left(t\right)=\Phi\left(t,t_0\right)P\left(t_0\right)\Phi^T\left(t,t_0\right)+\int_{t_0}^{t}\Phi\left(t,t'\right)G\left(t'\right)Q\left(t'\right)G^T\left(t'\right)\Phi^T\left(t,t'\right)dt' \tag{3.43}$$

The Kalman filter algorithm is comprised of five equations. First the state and covariance are predicted for the current time by

$$\hat{x}_k\left(-\right)=\phi\left(t_k,\hat{x}_{k-1}\left(+\right),t_{k-1}\right) \tag{3.44}$$

$$P_k\left(-\right)=\Phi_{k-1}P_{k-1}\left(+\right)\Phi_{k-1}^T+N_{k-1} \tag{3.45}$$

Next the Kalman gain matrix is found by

$$K_k=P_k\left(-\right)H_k^T\left[H_kP_k\left(-\right)H_k^T+R_k\right]^{-1} \tag{3.46}$$

Once a sensor measurement is received, the predicted state estimate and covariance matrix are corrected using

$$\hat{x}_k\left(+\right)=\hat{x}_k\left(-\right)+K_k\left[z_k-h\left(\hat{x}_k\left(-\right)\right)\right] \tag{3.47}$$

$$P_k\left(+\right)=\left(I-K_kH_k\right)P_k\left(-\right) \tag{3.48}$$

In equations 3.44 through 3.48 $(-)$ represents the a-priori estimate that has yet to be updated by a sensor measurement while $(+)$ represents a the a-posteriori estimate that is optimal. In addition k is the discrete time index and z is a sensor measurement, which is related to the state by

$$z_k=h\left(x_k\right)+v_k \tag{3.49}$$

where h is a system dependent function of x and v is sensor noise. The sensor noise is assumed to be white and gaussian such that

$$\begin{aligned} E\{v_k\} &= 0 \\ E\left\{v_k v_k^T\right\} &= R_k \delta_{kk'} \end{aligned} \tag{3.50}$$

The matrix H in equation 3.46 is given by

$$H_k = \left.\frac{\partial h(x)}{\partial x}\right|_{\hat{x}_k(-)} \tag{3.51}$$

3.3 Star Sensor Covariance

The covariance of the quaternion measurement error of the star sensor is necessary for use in the Kalman Filter. This covariance can be found for a specific, stationary satellite orientation in space by running a long simulation and numerically calculating the covariance of the quaternion error. However, using an analytic method yields a dynamic covariance matrix that changes with the attitude quaternion and thus can be used during attitude slews.

For a given set of star sensors and observation stars the covariance matrix of yaw, pitch, and roll is constant, and it can be determined. Lerner presents a procedure for translating the raw measurement covariance matrix into the covariance matrix for a quantity derived from the raw measurement [11]. In this case the procedure translates the yaw, pitch, and roll measurement covariance matrix into a quaternion error covariance matrix.

If the measurement error is small then the quaternion error can be related to the measurement error by expanding the quaternion error in a first-order Taylor series. This is shown mathematically in equation 3.52, where q_i is the i^{th} quaternion component, θ_y is yaw angle, ψ_p is pitch angle, and ϕ_r is roll angle.

$$\delta q_i = \frac{\partial q_i}{\partial \theta_y}\delta\theta_y + \frac{\partial q_i}{\partial \psi_p}\delta\psi_p + \frac{\partial q_i}{\partial \phi_r}\delta\phi_r \tag{3.52}$$

Equation 3.52 can be written as

$$\delta q = H'\delta y \tag{3.53}$$

where q is the quaternion array, y is an array in the order of yaw, pitch, roll, and H' is a 4×3 matrix of partial derivatives. The expected value of the quaternion error is

$$E\left\{\delta q \delta q^T\right\} = H' E\left\{\delta y \delta y^T\right\} H'^T \tag{3.54}$$

which can be written as

$$R_q = H' R_y H'^T \tag{3.55}$$

The matrix R_y is given by

$$R_y = \begin{bmatrix} \sigma^2_{\theta_y} & 0 & 0 \\ 0 & \sigma^2_{\psi_p} & 0 \\ 0 & 0 & \sigma^2_{\phi_r} \end{bmatrix} \tag{3.56}$$

where $\sigma^2_{\theta_y}$, $\sigma^2_{\psi_p}$, and $\sigma^2_{\phi_r}$ are respectively the variance of yaw, pitch, or roll for a given set of star sensors and observed stars. The diagonal form of R_y indicates an assumption that yaw, pitch, and roll are independent; however it will be shown in subsection 5.2.1 that this assumption is not always valid. Simulations have shown that when there are 2 or more stars on 2 or more FGS CCD's that the assumption is reasonable. When these quantities are not independent the off-diagonal terms can be found by simulation and numeric calculation.

The rotation matrix can be related to yaw, pitch, and roll angles by equation 3.57.

$$A = \begin{bmatrix} \cos\psi_p \cos\theta_y - \sin\theta_y \sin\psi_p \sin\phi_r & \cos\psi_p \sin\theta_y + \sin\phi_r \sin\psi_p \cos\theta_y & -\cos\phi_r \sin\psi_p \\ -\cos\phi_r \sin\theta_y & \cos\phi_r \cos\theta_y & \sin\phi_r \\ \sin\psi_p \cos\theta_y + \sin\phi_r \cos\psi_p \sin\theta_y & \sin\psi_p \sin\theta_y - \sin\phi_r \cos\psi_p \cos\theta_y & \cos\phi_r \cos\psi_p \end{bmatrix} \tag{3.57}$$

Using a small angle approximation and comparing equation 3.57 to 1.5 it can be found that

$$\begin{aligned} q_1 &\approx \tfrac{1}{2}\theta_y \\ q_2 &\approx \tfrac{1}{2}\psi_p \\ q_3 &\approx \tfrac{1}{2}\phi_r \\ q_4 &\approx 1 \end{aligned} \tag{3.58}$$

Equation 3.58 yields

$$H' = \begin{bmatrix} 0.5 & 0 & 0 \\ 0 & 0.5 & 0 \\ 0 & 0 & 0.5 \\ 0 & 0 & 0 \end{bmatrix} \tag{3.59}$$

This small angle approximation provides for a translation from yaw, pitch, and roll covariance into a quaternion representation that is relative to satellite body coordinates. Next this quaternion must be rotated to obtain the quaternion covariance relative to the reference coordinate system. The quaternion rotation is given by equation 1.10. The covariance matrix of the attitude quaternion can be found using equation 3.60

$$R = Q' R_q Q'^T \tag{3.60}$$

where

$$Q' = \begin{bmatrix} q'_4 & q'_3 & -q'_2 & q'_1 \\ -q'_3 & q'_4 & q'_1 & q'_2 \\ q'_2 & -q'_1 & q'_4 & q'_3 \\ -q'_1 & -q'_2 & -q'_3 & q'_4 \end{bmatrix} \tag{3.61}$$

In equation 3.61 q' is the quaternion measured by the star sensor. To be more exact q' should be the true attitude quaternion, but this information is not known. The desired star sensor covariance matrix for use in the Kalman filter equation 3.46 is R that is given in equation 3.60.

3.3.1 Applying the Kalman Filter to SNAP

The Kalman filter is used on SNAP to blend the SIRU measurements with the star sensor measurements to obtain a superior attitude estimate. To mesh information from the various sensors the period of output was set equal for the SIRU, Ball 602 star trackers, fine guiding sensor, and Kalman filter.

$$\Delta t_g \equiv \Delta t \equiv \Delta t_{KF} \equiv 0.1\,\text{sec} \tag{3.62}$$

The value of 10 Hz was chosen for this study. An optimization study was not performed on the sample frequency because it is assumed that system dynamic resonances and actuator control bandwidth will strongly dominate the choice of sample frequency.

For the Kalman filter the attitude is parameterized in terms of the 4-component quaternion. As mentioned in subsection 2.2.3 the gyroscope accumulates a bias in its measurements of body x, y, and z angular velocity. The Kalman filter is used to estimate and remove this bias so that the gyroscope measurements remain uncorrupted. The state vector for the system is thus comprised of seven components: the 4 components of the attitude quaternion and the 3 components of the SIRU bias.

$$x = \begin{bmatrix} q_1 & q_2 & q_3 & q_4 & b_x & b_y & b_z \end{bmatrix}^T \tag{3.63}$$

As follows from equation 2.12, 2.13, and 3.19 the dynamic equations of state are

$$\frac{d}{dt}q(t) = \frac{1}{2}\Omega\left(\omega_{meas}(t) - b(t) - \eta_1(t)\right)q(t) \tag{3.64}$$

$$\frac{d}{dt}b(t) = \eta_2(t) \tag{3.65}$$

The state error vector satisfies equation 3.38, with

$$F(t) = \begin{bmatrix} \frac{1}{2}\Omega(\hat{\omega}) & -\frac{1}{2}\Xi(\hat{q}) \\ 0_{3\times4} & 0_{3\times3} \end{bmatrix} \tag{3.66}$$

$$G(t) = \begin{bmatrix} -\frac{1}{2}\Xi(\hat{q}) & 0_{4\times3} \\ 0_{3\times3} & I_{3\times3} \end{bmatrix} \tag{3.67}$$

$$w(t) = \begin{bmatrix} \eta_1(t) \\ \eta_2(t) \end{bmatrix} \tag{3.68}$$

where η_1 and η_2 are the noise associated with the SIRU as defined by equations 2.12 through 2.16. The matrix Ξ is defined by

$$\Xi(q) = \begin{bmatrix} q_4 & -q_3 & q_3 \\ q_3 & q_4 & -q_1 \\ -q_2 & q_1 & q_4 \\ -q_1 & -q_2 & -q_3 \end{bmatrix} \tag{3.69}$$

The matrix Q from equations 3.30, 3.42, and 3.43 is given by

$$Q(t) = \begin{bmatrix} Q_1(t) & 0_{3\times3} \\ 0_{3\times3} & Q_2(t) \end{bmatrix} \tag{3.70}$$

where Q_1 and Q_2 are 3×3 matrices for the covariance of η_1 and η_2 respectively:

$$Q_1(t) = \begin{bmatrix} \sigma_v^2 + \frac{1}{\Delta t}\sigma_e^2 & 0 & 0 \\ 0 & \sigma_v^2 + \frac{1}{\Delta t}\sigma_e^2 & 0 \\ 0 & 0 & \sigma_v^2 + \frac{1}{\Delta t}\sigma_e^2 \end{bmatrix} \tag{3.71}$$

$$Q_2(t) = \begin{bmatrix} \sigma_u^2 & 0 & 0 \\ 0 & \sigma_u^2 & 0 \\ 0 & 0 & \sigma_u^2 \end{bmatrix} \tag{3.72}$$

Because the star sensors output the attitude quaternion the function h in equation 3.49 is simply equal to the true quaternion and v is the noise associated with this measurement. It follows that R is the covariance of the combined star sensor measurements from the *q-method*. Thus the matrix H in equation 3.46 is the following 4×7 matrix:

$$H_k = \begin{bmatrix} I_{4\times4} & 0_{4\times3} \end{bmatrix} \tag{3.73}$$

The 4×4 covariance matrix R is found by running a long simulation using only the star sensors and then calculating the attitude covariance in terms of yaw, pitch and roll. The analytic relationship to convert this covariance matrix into a quaternion covariance was derived in subsection 3.3.

To begin the simulation the initial state estimate is set equal to the true state. The SIRU bias is set to $[0, 0, 0]^T$. The covariance matrix, P, is initialized as a matrix of zeros. Evaluation of equation 3.43 is difficult, so the propagation of the covariance matrix for equation 3.45 is done by numerically integrating the Riccati equation 3.42 using a classical 4^{th} order Runge-Kutta method. The state propagation of equation 3.44 is done using the SIRU measurement with equation 3.26.

Chapter 4

Requirements and Simulation

4.1 Requirements

The pointing requirements on the SNAP ACS are considerably tight. It is necessary to hold the satellite extremely still while the telescope is taking an exposure of the sky. The science mission intends to make measurements on supernovae that lie at the edge of the known universe. For these targets a small error in pointing angle translates into an enormous distance error and could seriously corrupt the science data.

The satellite will operate in several modes, and the pointing requirements vary between each mode. The primary purpose of this ACDS study is to determine how well the satellite can point in each of its modes. The modes of operation are the following [5]:

1. Science Mode
   For 1000 seconds the telescope must be held very still as it collects science data from supernovae. During this time all sensors are available. The pointing requirements are as follows:

Table 4.1: Science Mode Requirements

Type	Requirement	Goal
Yaw/Pitch	0.02 arcsec RMS	0.01 arcsec RMS
Roll	0.80 arcsec RMS	0.40 arcsec RMS

2. Readout/Dither
   This is a 30 second period of time between the 1000 second science exposures during which the telescope makes small pointing changes. During this period the fine guiding sensor is not operational while the science-taking CCDs are being read-out and discharged. A shutter closes to block the path of light to the focal plane. The satellite must guide off of only the 3 Ball 602 star trackers and the SIRU during this mode. During the 30 seconds the satellite orientation is must satisfy the less strict requirements in table 4.2; however, once the 30 seconds ends and the shutter reopens then 2 seconds are allowed for the satellite to settle to its new target within the Science

Mode requirements. The move to the new target is between 0.25 and 1 arcsecond away from the previous target.

Table 4.2: Readout/Dither Mode Requirements

Type	Requirement	Goal
Yaw/Pitch	0.25 arcsec RMS	0.025 arcsec RMS
Roll	8.0 arcsec RMS	0.8 arcsec RMS

3. Readout/Dither with Cassegrain
   This scenario is the same as the Readout/Dither scenario, but the Cassegrain guider is now made available when the shutter is closed. The Cassegrain guider will be included on SNAP if the 2 second settling requirement cannot be met using only the Ball 602's and the SIRU.

4. Change of Pointing Direction
   This scenario encompasses several sizes of larger maneuvers. The shutter is closed and the FGS is unavailable. For all of the sizes of movement the satellite must be able to point within a 3×3 arcsec box with 98% confidence. Each size of movement has a different settling time requirement as shown in table 4.3

Table 4.3: Large Movement Requirements

Step Size	Settling Time
3 Arcminutes	30 Seconds
1 Degree	2 Minutes
15 Degrees	6 Minutes
180 Degrees	60 Minutes

In order to meet the requirements specified above, the precision of the measurements coming from the sensors must be higher than the goal for the overall system. Investigations are performed to determine the effectiveness of different combinations of sensors for each scenario in order to determine which sensors are necessary to meet the requirements. In cases where the SIRU is removed the Kalman filter is also removed, and guiding depends solely on the star sensors and the *q-method*.

4.2 The Simulation Loop

The attitude determination simulation was coded in Matlab for development and testing, after which it was coded into the larger control system simulation in C++. The flow of the simulation is summarized in figure 4.2.

At the top of the program loop the system parameters are specified. The universal time step is set to 0.1 seconds. The focal lengths of the FGS and Ball 602's are set to 21.66 and 0.085 meters respectively. The inertial properties of SNAP are set by specifying the mass

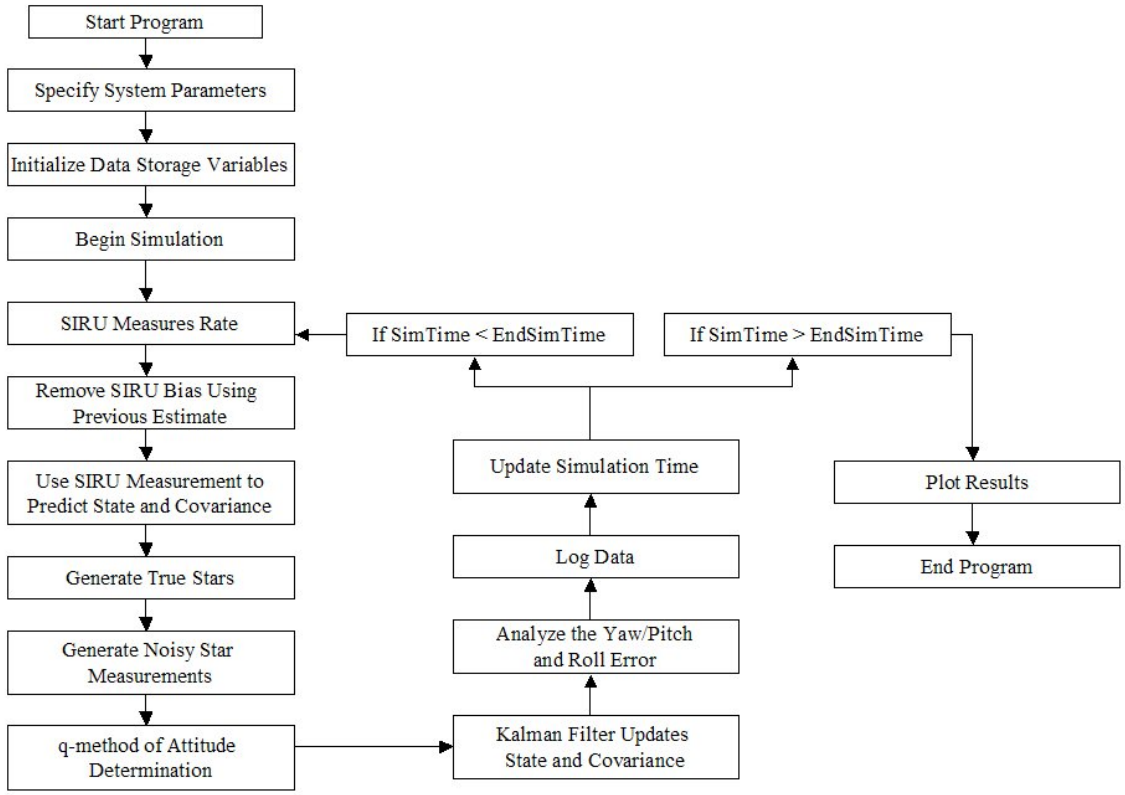

Figure 4.1: The program loop

as 1600 kg and the principle moments of inertia as $I_{xx} = 3200kg - m$, $I_{yy} = 3400kg - m$, $I_{zz} = 1200kg - m$. The principle moments of inertia are aligned with the satellite body X, Y, and Z axes as denoted by the subscripts. The FGS CCDs are set to be 0.0105 m by 0.0105 m and placed on the satellite X-Y plane in a square pattern where the center of each CCD is placed at a given angle from the satellite Z-axis. The magnitude of stars observed on the CCD is assumed to be 16 for this study. Using the sample rate and star brightness the standard deviation of stars on the FGS is calculated using equation 2.4. The Ball 602 star trackers are placed on the side of the spacecraft and oriented at various angles. The angular standard deviation of stars on the Ball 602's is set to 1.5 arcseconds. The number of stars to be seen by each sensor is set; the accuracy of the star sensors increases with the number of observation stars.

Several parameters are varied for investigation. The FGS CCD displacement angle from the Z-axis is varied between 0.35 and 0.7 degrees. The orientations of the Ball 602 star trackers are varied. The number of stars on the FGS is varied between 0 and 4, and the number of stars on each Ball 602 is varied between 1 and 5.

The initial conditions are then specified. Because different sensor combinations are to be investigated, the SIRU, FGS, and any or all of the Ball 602 star trackers can be toggled on or off. Because the Kalman filter uses the SIRU measurement in place of a dynamic model the Kalman filter estimation algorithm is not executed unless the SIRU is toggled on. The beginning quaternion is chosen arbitrarily, and the initial state estimate is set equal to the true state. If the SIRU is on then the bias is set to a vector of zeros and the covariance matrix is initialized to a matrix of zeros. The simulation is then started to run to a specified length of time.

In the Matlab simulation a small random zero-order hold torque is generated to make an angular velocity that constantly jitters the satellite orientation. In C++ a torque is generated by the control system to hold a position or to make a given maneuver.

The first attitude measurement is output from the combined star sensors. At program initialization stars are generated for the FGS and the Ball 602's. A star is created as a point on the 2-dimensional CCD surface. The point is constructed from 2 random variables where 1 random variable describes the X-coordinate on the CCD and the other describes the Y-coordinate. Each random varible has a uniform distribution over the width of the CCD in its respective coordinate. The planar point is made into a star vector observation by adding the focal length as the depth coordinate. The star vector is thus created in satellite body coordinates after which it is translated into inertial coordinates using the current rotation matrix via equation 1.1. At each time step the star in inertial coordinates is translated back into body coordinates to find its new position on the CCD. If a given star point has moved out of the range of the CCD then a new star is generated. In this way stars are allowed to move in discrete steps on the CCD, but the specified number of stars always exists on a given sensor. The star spots are assumed to be stationary over the sample period.

A star measurement is made by adding noise to the true star point on the CCD. To generate noise the radial distance of the noisy point from the true point is a random variable with gaussian distribution and a standard deviation specified by equation 2.4 for the FGS and 1.5 arcseconds for the Ball 602's. This angular standard deviation is translated into a linear distance using the focal length and equation 2.1. The angle of the noisy star spot about the true star spot is a random variable with uniform distribution from 0 to 360 degrees. As for the true star spot the 2-dimensional noisy star measurement is made into a 3-dimensional star vector by adding the focal length of the sensor as the depth coordinate.

The measured attitude is generated using the *q-method* with the measured star vectors in satellite body coordinates and the identified true stars in inertial coordinates as described in section 3.1. The measured star vectors from the Ball 602's and the FGS are weighed differently according to equation 3.18. The quaternion output from the *q-method* is normalized and input to the Kalman filter algorithm.

The SIRU simulation begins with the propagation of the true attitude. In Matlab the true attitude quaternion is propagated based on the average angular velocity over the time step. The angular velocity over the time step is set using the zero-order hold torque and a 4^{th} order Runge-Kutta ODE solver. At each time step within the Runge-Kutta solver the angular velocity is logged, and the values are averaged over the entire time step. The

attitude quaternion is then propagated using this averaged angular velocity in equation 3.26, and the new quaternion is normalized.

The simulation in C++ models a rigid body in 3-dimensional motion, and the attitude is simply output at any given time. The details of the model are beyond the scope of this report. The C++ simulation is not programmed to output average angular velocity over the time step. A close approximation for the average angular velocity can be obtained from the change in quaternion over the time step using equation 3.27.

The true change in pointing angle, θ_{true}, is created by numerical integration of the average angular velocity over the time step. A SIRU measurement is generated by first adding noise to θ_{true} using equation 2.31 and then differentiating and subtracting out the estimated bias using equation 2.32. The new quaternion is predicted by plugging the measured angular velocity into equation 3.26.

The SIRU-predicted quaternion constitutes the first step of the Kalman filter. The SIRU bias estimate remains constant until the after the next Kalman filter update. The second step is the propagation of the covariance matrix via numeric integration of the Riccati equation 3.42 using a classical 4^{th} order Runge-Kutta method. The Q matrix in equation 3.42 is specified using equations 3.70, 3.71, and 3.72. The Kalman filter gain matrix is next calculated using equation 3.46 where the covariance matrix, R, for the star sensor measurement is determined as described in section 3.3. The state estimate is updated using the Kalman gain matrix, K, in equation 3.47, where H is specified as in equation 3.73. The final step of the Kalman filter is to update the covariance matrix using equation 3.48. The estimated quaternion must again be normalized by its magnitude.

The next step of the simulation is to calculate the yaw/pitch and roll error associated with the current attitude estimate. To this end the quaternion is first translated into a rotation matrix.

The yaw/pitch error is found by the following steps: first rotate the body Z-axis vector, $[0, 0, 1]^T$, into reference coordinates using the true rotation matrix. Next use the measured, noisy rotation matrix to rotate the true Z-axis vector back into body coordinates. The error in the measured rotation matrix causes the true Z-axis vector to be slightly different than $[0, 0, 1]^T$ in the measured body coordinate system. The angular difference is the yaw/pitch error with respect to the true satellite body coordinates. This algorithm is illustrated by equations 4.1 through 4.3.

$$\vec{Z}_{true,i} = A_{true} \begin{bmatrix} 0 & 0 & 1 \end{bmatrix}^T \tag{4.1}$$

$$\vec{Z}_{meas,b} = A_{meas}^{-1} \vec{Z}_{true,i} \tag{4.2}$$

$$e_{yp} = \cos^{-1} \left(\frac{\vec{Z}_{meas,b} \cdot \begin{bmatrix} 0 & 0 & 1 \end{bmatrix}^T}{\left| \vec{Z}_{meas,b} \right|} \right) \tag{4.3}$$

where $\cdot$ denotes a dot product, $\vec{Z}_{true,i}$ is the Z-axis vector in inertial coordinates, $\vec{Z}_{meas,b}$ is the measured Z-axis vector in true body coordinates, A_{true} is the true rotation matrix, A_{meas} is the measured rotation matrix, and e_{yp} is the yaw/pitch error.

Roll is can be determined using the body X-axis vector, $[1,0,0]^T$. First the true X-axis vector is rotated into reference coordinates using the rotation matrix. Then this X-axis vector in reference coordinates is rotated to the measured body coordinates using the measured rotation matrix. The roll error is the angular difference between the true body X-axis vector, $[1,0,0]^T$, and the projection of the measured X-vector onto the true body X-Y plane. The calculation is performed using equations 4.4 through 4.6.

$$\vec{X}_{true,i} = A_{true} \begin{bmatrix} 1 & 0 & 0 \end{bmatrix}^T \tag{4.4}$$

$$\vec{X}_{meas,b} = A_{meas}^{-1} \vec{X}_{true,i} \tag{4.5}$$

$$e_{roll} = \cos^{-1}\left(\frac{\vec{X}_{meas,b} \cdot \begin{bmatrix} 1 & 0 & 0 \end{bmatrix}^T}{\left| \vec{X}_{meas,b} \right|} \right) \tag{4.6}$$

where $\vec{X}_{true,i}$ is the X-axis vector in inertial coordinates, $\vec{X}_{meas,b}$ is the measured X-axis vector in true body coordinates, and e_{roll} is the roll error.

Once calculated, the attitude determination errors are recorded. The simulation updates the time step, and the whole program loop is repeated.

4.3 SIRU Sample Rate Optimization

As shown in section 2.2.3 the SIRU rate measurement variance is found by squaring equation 2.11. After plugging in for the individual terms the variance is

$$\sigma^2[arcsec^2] = \frac{0.5\,(AWN)^2}{\Delta t} + (60ARW)^2\,\Delta t + \frac{(RRW)^2\,(\Delta t)^3}{12} \tag{4.7}$$

where the units on AWN, ARW, and RRW are [arcsec/Hz$^{1/2}$], [deg/hr$^{1/2}$], and [arcsec/s$^{3/2}$] respectively.

Differentiating with respect to Δt and setting the result equal to 0 yields an equation that can be solved for the sample rate that gives the minimum gyro variance. The optimal sample rate is 0.412 seconds at which the variance is $2.9703e^{-5}$ arcsec^2. At the current system-wide sample rate of 0.1 seconds the SIRU variance is $6.485e^{-5}$ arcsec^2. Figure 4.2 plots the variance as a function of sample period.

Although the SIRU variance is minimized at a sample period of 0.412 seconds this optimal system-wide sample rate remains undetermined and depends heavily on the controller design that is not considered here.

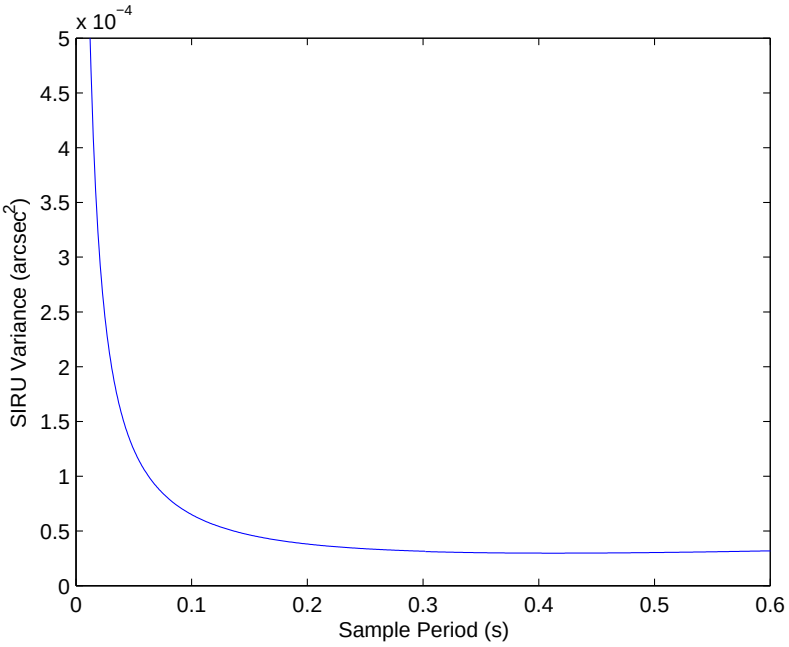

Figure 4.2: SIRU variance vs sample period

Chapter 5

Results

Several parameters are varied in order to determine their effect on the satellite's pointing capabilities. The position of the FGS CCDs is tested at between 0.35 degrees and 0.7 degrees. The number of stars on the FGS is varied, as well as which CCDs of the FGS observe the stars. The FGS is tested alone, with the Ball 602's, with the SIRU, and with both SIRU and Ball 602's. The Ball 602's are tested both alone and with the SIRU. The number of stars observed by each Ball 602 is varied. Several tests are run to determine the capabilities of the Ball 602's in the case any 1 of them fails. A test is run to determine the rate of degradation of the SIRU measurements when starting from a perfect measurement. An additional test is run to determine the expected value of attitude error after a 30 second period of guiding off of the SIRU combined with the Ball 602's. For this test the initial state estimate is provided by first simulating a 10 second period during which the FGS, Ball 602's and SIRU are all operating. At the end of 10 seconds the FGS is switched off and the attitude estimate becomes increasingly less accurate as time progresses. The FGS is left off for 30 seconds to simulate the closed-shutter scenario.

5.1 Ball 602 Orientation and Redundancy

An investigation was performed to determine the necessary number and orientation of Ball 602 star trackers. Of concern is the pointing ability of the spacecraft if any 1 of these commercial sensors fails. This redundancy issue is critical during modes in which the FGS is unavailable. In this scenario attitude estimation is provided by the SIRU and Ball 602s. The 602s can only provide an attitude estimate if they observe at least 2 star vectors. Because a single Ball 602 can track up to 5 stars at once the 2 necessary star vectors could potentially be obtained by 1 sensor. Alternatively, the 2 stars could be provided by 2 separate 602 sensors. The wide field of view of the star trackers ensures at least 1 guide star per tracker. After observing the results produced using the maximum of 5 stars on each star tracker, the number of star per tracker was reduced to 1 to model the worst case.

The scenarios that were simulated for this study are shown in tables 5.1 through 5.6. The orientations of 2-3 potential star trackers were varied in 3 tests: in the first the 3 star

trackers were placed each 120° from one another, in the second the star trackers were placed orthogonally at 90° from one another, and in the third 2 trackers were placed 45° from one another while the third was placed orthogonal to both. Simulations of the nominal 30 second closed shutter period were performed both with and without the aid of the SIRU. In addition, simulations of various length were performed using the SIRU alone in which the initial orientation estimate is provided by a high accuracy FGS + Kalman filter solution. The most minimal simulation determined attitude using 2 stars on a single Ball 602 star tracker.

Table 5.1: Ball 602 Pointing Error: 5 stars on each star tracker, no SIRU

Orientation	Error Type	All Three 602s	Worst of any Two 602s
$120° - 120° - 120°$			
	Yaw/Pitch	0.74 arcsec RMS	1.15 arcsec RMS
	Roll	0.38 arcsec RMS	0.55 arcsec RMS
$90° - 90° - 90°$			
	Yaw/Pitch	0.76 arcsec RMS	1.05 arcsec RMS
	Roll	0.38 arcsec RMS	0.50 arcsec RMS
$45° - 45° - 90°$			
	Yaw/Pitch	0.81 arcsec RMS	1.39 arcsec RMS
	Roll	0.35 arcsec RMS	0.51 arcsec RMS

Table 5.2: Ball 602 Pointing Error: 1 star on each star tracker, no SIRU

Orientation	Error Type	All Three 602s	Worst of any Two 602s
$90° - 90° - 90°$			
	Yaw/Pitch	1.06 arcsec RMS	1.51 arcsec RMS
	Roll	0.78 arcsec RMS	1.05 arcsec RMS

Table 5.3: Ball 602 Pointing Error: 1 star on each star tracker + SIRU for 30 seconds

Orientation	Error Type	All Three 602s	Worst of any Two 602s
$90° - 90° - 90°$			
	Yaw/Pitch	0.25 arcsec	0.35 arcsec
	Roll	0.25 arcsec	0.35 arcsec

Table 5.4: Ball 602 Pointing Error: 2 stars on a single star tracker, no SIRU

Orientation	Error Type	Error Value
Aligned with Body Z-axis		
	Yaw/Pitch	1.10 arcsec RMS
	Roll	24.24 arcsec RMS

Table 5.5: Ball 602 Pointing Error: 2 stars on a single star tracker + SIRU for 30 seconds

Orientation	Error Type	Final Error
Aligned with Body Z-axis		
	Yaw/Pitch	0.51 arcsec
	Roll	0.55 arcsec

Table 5.6: SIRU only: Pointing error at the end of various time lengths

Time Length	Error Type	Final Error
30		
	Yaw/Pitch	0.55 arcsec
	Roll	0.55 arcsec
300		
	Yaw/Pitch	1.5 arcsec
	Roll	1.5 arcsec
1000		
	Yaw/Pitch	3 arcsec
	Roll	3 arcsec

The cases that involve SIRU measurements show results for the worst case observed over several simulations. Because the SIRU measurements have 2 distinct drift components the measurement error varies substantially between individual simulations. In some cases the SIRU measurements remain very accurate when the periods of negative drift are approximately equal to the periods of positive drift. The worst-observed scenarios displayed in tables 5.1 through 5.6 show results for the infrequent simulations in which SIRU drift moved steadily in either the positive or negative direction. On average the SIRU will perform much better than the accuracies reported in the tables.

Because the results of table 5.1 indicate that an orthogonal arrangement provides the best redundancy the orthogonal arrangement was chosen as the baseline. Furthermore, simulations showed that the orientation of 3 orthogonal star trackers with respect to the satellite body is does not affect pointing error.

The scenario involving 2 stars on only 1 tracker displays very poor roll accuracy relative to the other scenarios. This single sensor does not provide the necessary distance between 2 star observations that is necessary to accurately determine roll. The observed poor roll accuracy agrees with the specifications given by Ball Aerospace thus indicating a valid simulation model.

The majority of simulation results displayed in tables 5.1 through 5.6 show that the pointing requirements of table 4.2 will not be satisfied. The only scenario that meets requirements is 3 orthogonal Ball 602s used in league with the SIRU. Use of the SIRU greatly increases pointing accuracy in all cases. It should be noted that the results shown here represent the worst-case for which the attitude determination is still operational; the pointing requirements of table 4.2 will generally be satisfied.

5.2 Additional Sources of Pointing Error

The SNAP pointing capabilities have been characterized based on star photon centroid noise on the fine guiding CCDs. The yaw/pitch pointing capabilities have been described in Secroun et al. based on the expected standard deviation of this centroid [13]. Two sources of additional error have been identified. The first comes from roll error, which is typically between 1 and 2 orders of magnitude less accurate than yaw/pitch error. Intuition may suggest that roll error should not affect yaw pitch error; however, because yaw/pitch is not derived from a star directly along the satellite Z-axis, roll error limits the ability to determine yaw/pitch. The second additional source of error is movement of the star on the CCD over the sample period during which photons are gathered. The range of star movement on the CCD is dependent on angular velocity of the satellite. The effect is that the photons are no longer normally distributed about a stationary mean but instead are blurred along the direction of star motion.

5.2.1 Roll Error and Stars Vectors Offset from the Z-axis

The roll error influence on yaw/pitch error is only a significant effect for the case of only 1 observed star on the fine guiders. It is anticipated that this scenario accounts for between 2% and 13% of the mission. Before examining the fine details of 3-dimensional attitude determination it is reasonable to think that yaw/pitch estimation and roll estimation are independent; however, rigorous simulation of SNAP ACS consistently showed a correlation between the 2. The details of the relationship became of interest during simulations where the position of fine guiding CCDs on the focal plane was varied. The simulations showed that as the CCDs were moved radially outward from the center of the focal plane that yaw/pitch error increased. This result was curious because the statistical noise of the star centroid on the CCD was held constant.

If the noise characteristics of the star used to determine the yaw/pitch are held constant why does the yaw/pitch error increase with CCD radius from the center of the focal plane?

The first step in understanding this behavior is to understand that 2 stars are needed to determine the attitude of the satellite. In the case of only 1 star on the focal plane the primary star is the star appearing on the fine guiding CCD. The secondary star is a star obtained from the Ball 602 star trackers, which are much less accurate than the fine guider CCDs.

The reason for the influence of roll error on yaw/pitch error lies in the attitude determination algorithm. The primary star vector is observed in satellite body coordinate, denoted by subscript b. The star is identified using a star catalogue, so same star vector is known in inertial coordinates. Aligning the star vector in body coordinates with the star vector in inertial coordinates specifies 2 of the 3 degrees of freedom of the orientation of the body coordinate system in inertial space. Roll about the star vector is unspecified without an additional star vector observation. Because it is supplied by the Ball 602 star trackers, this secondary star vector is an order of magnitude less accurate than the primary star vector.

If the primary star vector was directly aligned with the Z-axis of the satellite then

yaw/pitch error would be fully specified by the primary star vector and unaffected by roll error. However, because the primary mirror of the telescope is an annulus, star vectors aligned with the Z-axis are not observed. The focal plane observes a donut-shaped region that lies between 0.35 and 0.7 degrees of tilt from the Z-axis. Due to this angular offset the yaw/pitch is not fully specified by the primary star vector and information from the secondary, less accurate, vector is needed.

The yaw/pitch dependency on the secondary vector increases with the angle by which the primary star vector is offset from the satellite Z-axis; therefore the yaw/pitch error increases with this angle. Based on the 3-dimensional geometry of the star observations and angular errors the theoretical effect of roll error on yaw/pitch error can be predicted using the following algorithm:

First the primary star vector is constructed as

$$\begin{gathered} v_1 = \left[\begin{array}{ccc} \tan(\theta_L) & 0 & 1 \end{array} \right] \\ v_1 = \frac{v_1}{|v_1|}, \end{gathered} \tag{5.1}$$

where θ_L is the angle between the star vector and satellite Z-axis. Next an error star vector is constructed at a slightly larger angle than θ_L as

$$\begin{gathered} v_2 = \left[\begin{array}{ccc} \tan(\theta_L + \gamma) & 0 & 1 \end{array} \right] \\ v_2 = \frac{v_2}{|v_2|}, \end{gathered} \tag{5.2}$$

where γ is the angular error of a star vector on the FGS. Next the error star vector is rotated in the X-Y plane to introduce the effect of roll error, which is denoted by e_{roll}. This is done by

$$\begin{gathered} v_2 = \left[\begin{array}{ccc} v_2(1)\cos(e_{roll}) & v_2(2)\sin(e_{roll}) & v_2(3) \end{array} \right]^T \\ v_2 = \frac{v_2}{|v_2|} \end{gathered} \tag{5.3}$$

The theoretical yaw/pitch error, α is now the angle between v_1 and v_2 found using a dot product denoted by $\cdot$

$$\alpha = \cos^{-1}(v_1 \cdot v_2) \tag{5.4}$$

The results of this theoretical prediction were plotted with actual simulation results for θ_L varying between 0.35 degrees and 0.7 degrees where roll error, e_{roll}, is held constant at 0.08 arcseconds. Figure 5.1 shows a high degree of accuracy between predicted and simulated behavior. It should be noted that the attitude determination algorithm as explained in section 3.1 is more intricate than the simple model used here to explain this behavior. To minimize yaw/pitch error the fine guider CCDs should be placed as close as possible to the center of the focal plane. The roll error only affects the yaw/pitch error in situations when there is only 1 star on the FGS. When there are 2 or more stars on 2 or more of the 4 FGS CCD patches then yaw/pitch is determined using multiple high accuracy star measurements. In this case the yaw/pitch error ceases to depend on the placement of the

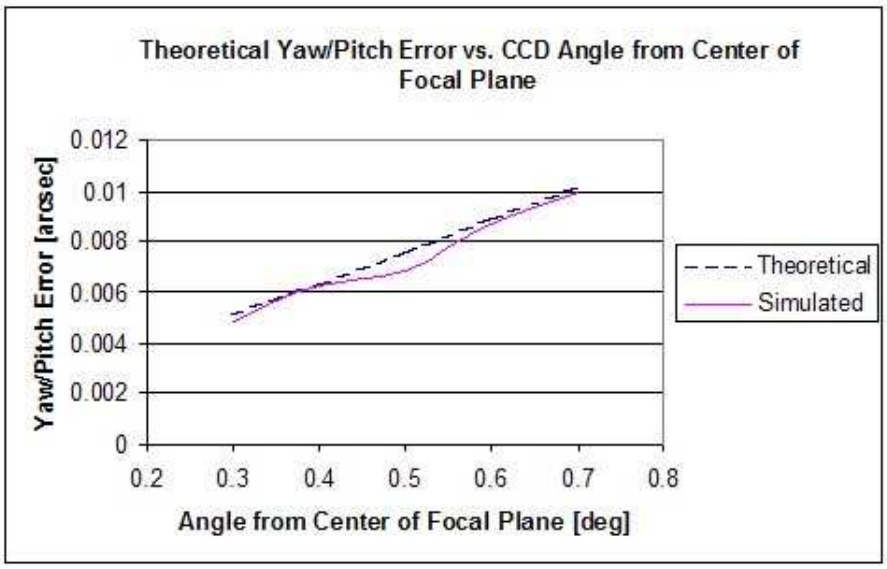

Figure 5.1: Relationship between focal plane guider position and yaw/pitch error

FGS CCDs. In addition, when 2 or more stars appear on 2 or more of the 4 FGS CCD patches then roll information can be obtained from the FGS. The FGS-determined roll is generally of higher accuracy than the Ball 602-determined roll.

An early pointing path investigation by Bradley and Markley revealed that there is an 83.57% chance of having more than 1 guide star on the FGS during the planned pointing path [3]. The planned pointing path has since been altered, and the study has not been repeated for the new path. It is estimated that there is a 97.6% chance of having 1 star on the FGS at any given time. Because instances of having a guide star on the FGS are independent events it is projected that there is a 95% chance of having 2 guide stars on the FGS.

5.2.2 Motion of Stars on the CCD

If the satellite is completely stationary individual photons from a single star will fall on the CCD with an approximately normal distribution of mean m and variance s^2. In reality the satellite will be rotating in space, and the star will not have a stationary mean. Instead the mean will follow a path on the CCD. Obviously the speed of the motion of the star centroid on the CCD will depend on the rotational velocity of the satellite. The potential error is higher when the satellite is dithering and when less accurate pointing induces a small constant motion.

Two questions are raised:

- How does a moving mean affect the centroid of photons over 1 sample period?
- During open shutter is the rotational velocity of the satellite significant enough to affect the star centroid?

Addressing Question 1:

A fundamental result from statistics is that the sum of several normally distributed random variables is a normally distributed random variable. The position at which each photon lands on the CCD can be considered an independent random variable, S_n, where n designates the n^{th} photon. The mean of the distribution of the star centroid, $S_{centroid}$, will be the mean of the N_p individual photons.

$$S_{centroid} = \frac{\sum_{n=1}^{n=N_p} S_n}{N_p} \tag{5.5}$$

For a qualitative analysis it is assumed that over the sample period, $t_s = 0.1sec$, the star centroid moves in a straight line. This is not a bad assumption during high-accuracy open-shutter mode. During the sample period the linear position of the star, $S(t)$, is specified by it the position at the beginning of the period, S_0, and a linear velocity, u, which is specified by the constant spacecraft spin rate.

$$S(t) = S_0 + ut \tag{5.6}$$

Using basic statistics the mean of the centroid can be shown to be half-way between S_0 and $S(t_s)$.

Because each photon is independent the standard deviation of the centroid will be unaffected by the velocity and is specified by equation 2.2 just as for the stationary case. Thus the centroid of a moving star will have a mean at the mean position of the star and have the same standard deviation as that for a stationary star.

Addressing Question 2:

The additional linear centroid position error added by velocity is equal to $0.5ut_s$ because the centroid lies at the average linear position over the sample period. To minimize this error either a faster sampling rate can be used or the velocity can be minimized. Assuming the centroid error for a motionless satellite is 0.005 arcseconds and the sample rate is 0.1 seconds then a velocity of 0.01 arcseconds/second would result in a 10% increase in centroid error.

Investigations are ongoing to determine the expected angular velocity during fine guiding mode. If this velocity is large enough to prevent achievement of the ACS pointing goal then solutions will be explored. One solution possibility is to use filtering to predict a star position at the end of the sampling period. A more simple solution is to place a velocity cap on the satellite controller so that it physically cannot move at a sufficient velocity to cause significant star blur.

5.3 Comparison of Simulation Results

Example plots of the yaw/pitch and roll error results for a simulation are shown in figures 5.2 and 5.3. In the figures each asterisk represents an individual value of the attitude error

at an individual time step. Because the sample rate is set to 10 Hz there are 10 data points per second. The RMS value is plotted as a line across the plot.

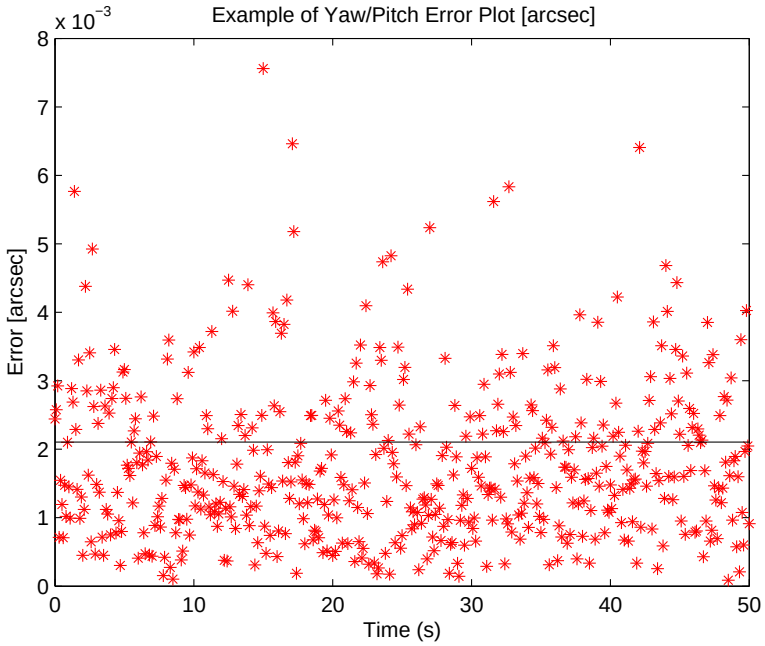

Figure 5.2: A typical plot of yaw/pitch error data.

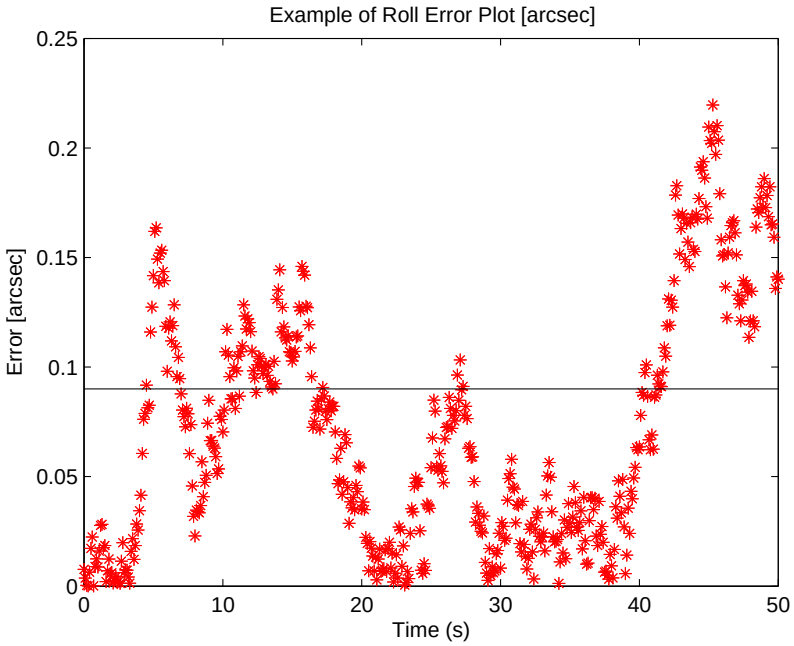

Figure 5.3: A typical plot of roll error data.

Table 5.7 displays steady state RMS attitude error results for some of the scenarios listed at the beginning of chapter 5. Scenarios 3 and 4 simulate a combination of sensors with 1 star observed on the FGS, 1 star on each of the 3 Ball 602's, and the SIRU. This represents the worst case scenario during science mode. As mentioned in subsection 5.2.1 the probability of having at least 1 star on the FGS is 97.6% while the probability of 2 stars is estimated to be 95%. It was also mentioned that yaw pitch error can be significantly smaller when multiple stars are observed on the FGS. This claim is supported by a comparison of scenarios 2 and 6. With only 1 FGS star, scenario 2 displays a yaw/pitch error of 0.0094 arcsec; however, the 2 FGS stars of scenario 6 drive the yaw/pitch error down to 0.0026 arcsec. As presented in subsection 5.2.1, with only 1 FGS star the yaw/pitch error increases as the offset of the FGS CCD's from the center of the focal plane increases; however the presence of an additional FGS star nullifies this effect and reduces yaw/pitch error significantly.

Table 5.7: Steady state RMS pointing error results for various FGS placement scenarios.

No.	Configuration	Yaw/Pitch [arcsec]	Roll [arcsec]
1	1 star on FGS at 0.35 deg + 1 star per Ball 602	0.0054	0.73
2	1 star on FGS at 0.7 deg + 1 star per Ball 602	0.0094	0.73
3	1 star on FGS at 0.35 deg + 1 star per Ball 602 + SIRU	0.003	0.3
4	1 star on FGS at 0.7 deg + 1 star per Ball 602 + SIRU	0.0045	0.3
5	2 stars on 2 FGS at 0.35 deg + 1 star per Ball 602	0.0026	0.32
6	2 stars on 2 FGS at 0.7 deg + 1 star per Ball 602	0.0026	0.18

The results for scenarios 1 and 2 indicate that when only 1 star is observed on the FGS fulfillment of the science mode goals as listed in table 4.1 is questionable. The results of scenarios 3 and 4 indicate that with the addition of the SIRU these pointing goals are exceeded.

The data in table 5.7 is useful for deciding where to place the FGS CCD's, between 0.35 and 0.7 degrees from the center of the focal plane. The science mode pointing goals listed in table 4.1 are significantly more strict in yaw/pitch (0.01 arcsec) than roll (0.4 arcsec). Comparing scenarios 3 and 4 from table 5.7 it can be seen that when only 1 star is observed on the FGS the movement of the FGS CCD's from 0.35 to 0.7 degrees results in a 50% increase in yaw/pitch error while the roll error remains constant. In contrast, scenarios 5 and 6 show that when multiple FGS stars are available placement of the CCD's at 0.7 degrees is in fact advantageous because yaw/pitch estimation is equally accurate while roll error is more accurate than that obtained from CCD's at 0.35 degrees.

The fact that the acceptable level of roll error is more than an order of magnitude greater than the acceptable level of yaw/pitch error suggests that the CCD's should be placed at 0.35 degrees to optimize yaw/pitch determination. However, the probability of only 1 star on the FGS is estimated to be 2.5% while the probability of 2 or more FGS stars is 95%. The probabilities indicate that placement of the CCD's at 0.7 degrees would result in a 50% decrease in yaw/pitch accuracy over 2.5% of the sky during the worst case scenario while the roll error be improved by at least 40% over 95% of the sky. By using the

SIRU the science mode goals can be met in either FGS configuration.

Table 5.8 displays data that communicates the trends obtained by varying sensor parameters. The data in table 5.8 was generated with FGS sensors placed at 0.35 degrees.

Table 5.8: Steady state RMS pointing error results.

No.	Configuration	Yaw/Pitch [arcsec]	Roll [arcsec]
7	2 stars on 1 FGS at 0.35 deg	0.15	24
8	2 stars on 2 FGS at 0.35 deg	0.0026	0.35
9	4 stars on 4 FGS at 0.35 deg	0.0015	0.18
10	1 star per Ball 602	1.06	0.78
11	5 stars per Ball 602	0.76	0.38
12	2 stars on 2 FGS at 0.35 deg + SIRU	0.0021	0.097
13	2 stars on 2 FGS at 0.35 deg + 1 star per Ball 602 + SIRU	0.0021	0.093
14	1 star per Ball 602 + SIRU	0.106	0.083

Scenarios 10 and 11 show the attitude determination capabilities of the 3 Ball 602 star trackers used without the FGS or SIRU. Scenario 10 was simulated with only 1 star per Ball 602. The Ball Aerospace specification for this instrument guarantees at least 1 star observed per sensor in any given orientation. Scenario 11 was simulated using 5 stars per tracker, the maximum number that can be simultaneously tracked. As expected, increasing the number of stars per sensor increases the overall accuracy. These results show that the science mode accuracy requirements cannot be met using only the Ball 602's; it is necessary to have at least 1 star on the FGS. In scenarios 10 and 11 the roll error is conspicuously smaller than yaw/pitch error. This is caused by the fact the roll error is found by projecting the measured X-axis onto the true XY plane and calculating the angle while the yaw/pitch error is calculated as a total 3-dimensional angle. Section 5.1 discussed the capabilities of the Ball 602's in the case of failure of any 1 of the 3 sensors.

Scenarios 7, 8 and 9 were simulated using only the fine guiding sensors. Scenario 7 shows that although attitude can be fully determined with 2 stars that fall on the same FGS CCD the measurement error is far outside of the range desired for the science mode. Scenarios 8 and 9 show that when multiple stars fall on multiple FGS CCD's the measurement accuracy increases dramatically, and in this case the Ball sensors do not improve the attitude estimate. Because the patches of sky seen by the 4 CCDs are not adjacent roll error can be determined rather accurately using 2 or more stars on 2 or more CCD's. When only 1 star is observed on the FGS the Ball sensors are necessary to fully determine the attitude. Comparing scenario 5 to 13 shows that when multiple FGS stars are available adding the SIRU still makes a large improvement in roll error, reducing it to 0.093 from 0.32 arcsec.

Scenario 13 was created to represent the typical sensor scenario for most satellite orientations. Multiple stars appear on the FGS, 1 star appears per Ball 602, and the SIRU is in use. The attitude determination accuracy during normal operation was found to be 0.0021 arcsec in yaw/pitch and 0.093 arcsec in roll.

The results of scenario 12 compared to those of scenario 13 show that the Ball sensors are of very little use during the motionless science mode under typical conditions.

Scenario 14 was simulated using only the Ball 602's and the SIRU. Using the Kalman filter at steady state this combination of sensors reaches the RMS values listed in table 5.8. These values apply for the case of a large satellite maneuver during which the FGS is not available. The time requirements for this case are listed in table 4.3. The requirement for the ADCS is to make the given maneuver to within a 3 by 3 arcsec box with 98% confidence. The data listed for scenario 14 indicates that this requirement is easily fulfilled.

Table 5.9 and figures 5.4, 5.5, 5.6, and 5.7 show results for non-steady state attitude determination.

Table 5.9: Non-steady RMS pointing error results.

No.	Configuration	Yaw/Pitch [arcsec]	Roll [arcsec]
14	1 star per Ball 602 + SIRU 30 sec	0.105	0.09

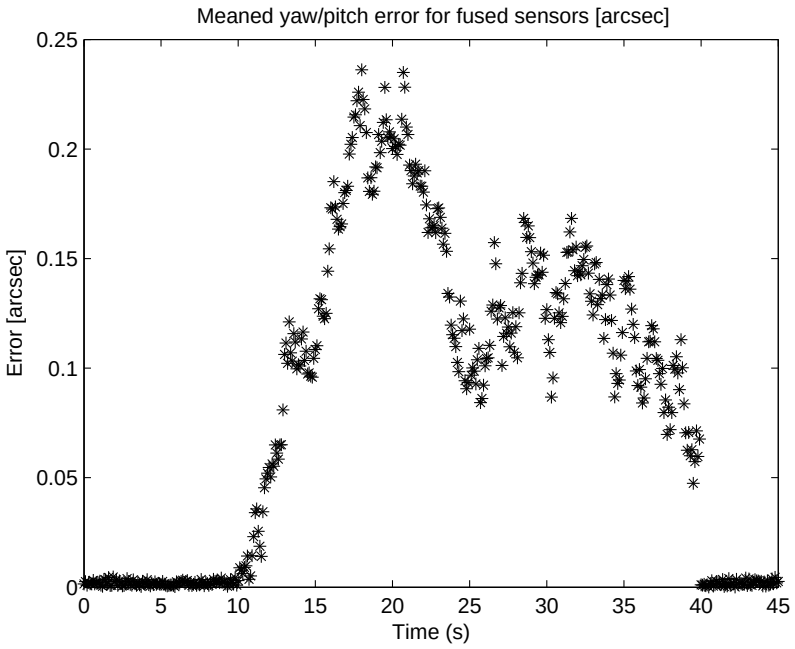

Figure 5.4: Yaw/Pitch error obtained when the FGS is turned off for 30 seconds.

Scenario 15 is a result showing the furthest the satellite can be expected to drift over the 30 second readout/dither mode when the FGS is unavailable. The random walk behavior of the SIRU can cause the attitude estimate error to either increase or decrease each time step. The data in table 5.9 was taken from the worst case observed over dozens of simulations; it represents the value of the error at the end of 30 seconds. In this specific case within the 30 seconds the sensor combination nearly reaches its steady state value given by scenario 14.

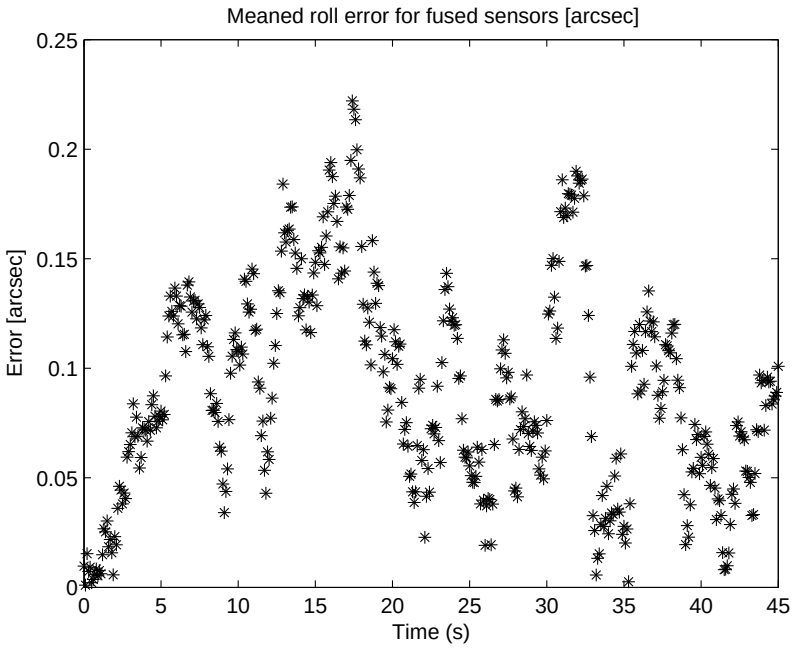

Figure 5.5: Roll error obtained when the FGS is turned off for 30 seconds.

This is much faster than the time a typical simulation takes to reach this steady state. An example of the behavior is plotted in figures 5.4 and 5.5. In these plots the FGS is on for the first 10 seconds at which point it is turned off and guiding relies on the SIRU and 602's. The FGS is turned on again at 40 seconds. The simulation revealed that the Ball 602's and SIRU are able to keep the attitude estimation comfortably within the goals listed in table 4.2. Results from the separate study of the control system indicate that starting from the attitude error of scenario 15 the control system can in fact settle the attitude to within the science mode requirement within 2 seconds, thus fully satisfying the goals associated with the readout/dither mode. If the SIRU were not used in this mode the accuracy would be that of scenario 10 and outside of the requirement.

Figures 5.6 and 5.7 show an example of SIRU-determined attitude drift in time while it is not corrected by the Kalman filter. As time increases the SIRU measurement becomes increasingly inaccurate. The random walk behavior of the SIRU-determined attitude is shown well by the combination of figure 5.6, in which the error steadily increases over time, and figure 5.7, in which the error both increases and decreases. The random walk noise can cause the error to move in either direction, but over a long enough time period the error will increase if the bias is not estimated and removed.

The results reported here are pure sensor results and do not include the additional error that is generated by other noise sources. Additional sources of error include the controller performance, actuator disturbances, structural flexibility, fuel slosh, and thermal effects on the structure and hardware.

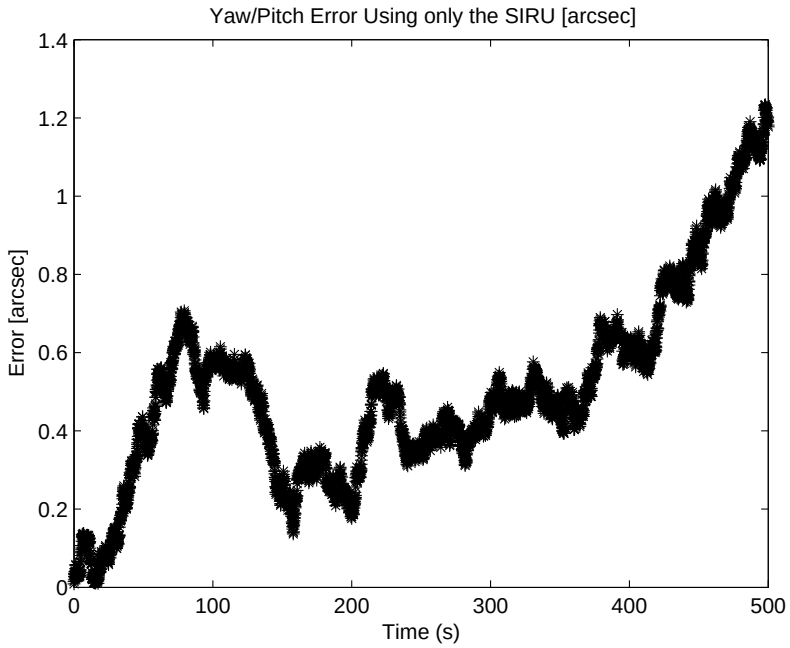

Figure 5.6: Yaw/pitch error obtained by using the SIRU alone.

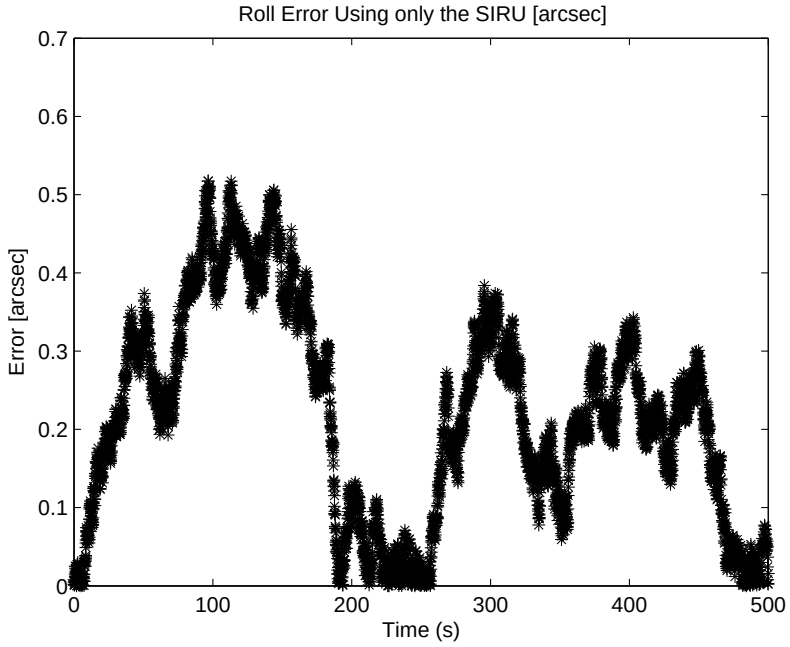

Figure 5.7: Roll error obtained by using the SIRU alone.

5.4 Conclusion

The proposed sensors for the SNAP satellite are able to satisfy the attitude determination requirements. The results of the ADS study as reported here show that the requirements during each operational mode of the spacecraft can be exceeded by using combinations of the fine guiding sensors, the Ball 602 star trackers, and the Northrop Grumman SIRU.

An extended Kalman filter has been developed to fuse distinct measurements from the SIRU and the star sensors in order to yield an optimal attitude estimate. Use of the SIRU and Kalman filter enable the requirements of the readout/dither mode to be satisfied while the Ball sensors alone are insufficient. The requirements of the large maneuver mode can be satisfied using only the 3 Ball 602's; however adding the SIRU and Kalman filter to the Ball sensors improves the steady state error by an order of magnitude. The performance of the Ball sensors and Kalman filter is accurate enough to make the cassegrain guider unnecessary, although the cassegrain guider would improve pointing accuracy while the telescope shutter is closed.

This investigation determined that the optimal arrangement of Ball 602 star trackers is orthogonal. This provide the best attitude accuracy when all 3 602's are operational as well as if any 1 fails.

During science mode the Ball sensors are necessary to determine attitude when fewer than 2 stars are observed by the FGS. In this scenario the SIRU and Kalman filter contribute greatly to the reduction of attitude error. When 2 or more stars are observed by 2 or more of the FGS CCD's then the Ball sensors add little to the attitude estimate. In this scenario the SIRU and Kalman filter still work to reduce the roll error to 1/3 of its value without the Kalman filter.

A typical science mode sensor scenario involves 2 stars on 2 FGS CCD's, 1 star on each of the Ball 602's, and an operational SIRU and Kalman filter. Simulation of this typical scenario indicate that the satellite has RMS sensing errors of 0.0021 arcsec in yaw/pitch and 0.093 arcsec in roll. When only 1 star is observed on the FGS this error can increase to as high as 0.0045 arcsec in yaw/pitch and 0.3 arcsec in roll.

The SNAP ACS team is working with the NASA supported simulation tool Treetops and a self coded near rigid model to simulate the overall control system. Working with 2 parallel and independent simulations provides a means to verify software as well as rule out implementation and coding errors

This study was conducted assuming a rigid satellite body, and it has neglected all sources of error other than that directly attributable to the SIRU and star sensors. The ADS results presented here form the foundation of the larger attitude control system study that will develop a more detailed satellite, its hardware, and its control system. Important issues that have not yet been addressed are the time delay of computing and actuation and computational lag of the sensors and Kalman filter. If the Kalman filter computation time is significant relative to the sample rate then the Kalman filter may be less useful.

Potential areas for further investigation include the optimization of the system wide sample rate, the accurate prediction of star motion on the FGS CCD's, and the modeling

of sensor noise modified by a flexible spacecraft. In addition the development of an accurate dynamic model of the spacecraft would enable a double Kalman filter in which the spacecraft motion predicted by the model could be blended with the SIRU rate measurement. The output of this first Kalman filter could then be blended with the star sensor attitude estimate using a second Kalman filter.

The satellite is scheduled to be launched in 2010. As work continues to progress on the Attitude Control Simulation a more extensive investigation of the parameter space will be conducted.

Bibliography

[1] Ball Aerospace and Technologies Corp. *CT-602 Star Tracker*, 2003. http://www.ball.com/aerospace/.

[2] Chris Bebek et al. "SNAP Satellite Focal Plane Development". Technical report, Lawrence Berkeley National Laboratory, U.C. Berkeley, 2003.

[3] Art Bradley and Landis Markley. "ISAL Study: SNAP Fine Guidance". PowerPoint presentation, Nov. 2001. http://snap.lbl.gov.

[4] R.L. Farrenkopf. "Analytic Steady-State Accuracy Solutions for Two Common Spacecraft Attitude Estimators". *Journal of Guidance and Control*, 1:282–284, Jul.-Aug. 1978.

[5] Henry Heetderks. "SNAP ACS Requirements". PowerPoint presentation, Space Sciences Laboratory, U.C. Berkeley, Apr. 2003. http://snap.lbl.gov.

[6] J. Keat. "Analysis of Least-Squares Attitude Determination Routine DOAOP". Technical Report CSC/TM-77/6034, Comp. Sc. Corp., 1977.

[7] Robin Lafever. S14-02. http://snap.lbl.gov.

[8] Michael Lampton, 2003. Private correspondence.

[9] Michael Lampton. "TMA62A". PowerPoint presentation, Space Sciences Laboratory, U.C. Berkeley, 2003. http://snap.lbl.gov.

[10] E.J. Lefferts, F.L. Markley, and M.D. Shuster. "Kalman Filtering for Spacecraft Attitude Estimation". *Journal of Guidance*, 5(5):417–429, Sept.-Oct. 1982.

[11] Gerald M. Lerner. "q method". In James. R. Wertz, editor, *Spacecraft Attitude Determination and Control*, chapter 12.2.3, pages 426–428. Kluwer Academic Publishers, 1978.

[12] Anuscheh Nawaz. "The Sensor System for Fine Guiding the SNAP Satellite". Master's thesis, The University of California at Berkeley, 2003.

[13] A. Secroun, M. Lampton, and M. Levi. "A high accuracy, small field of view star guider with application to SNAP". *Experimental Astronomy*, 11, June 2002.

[14] Spence, Jr., C.B., and Markley, F.L. "Attitude Propagation". In James. R. Wertz, editor, *Spacecraft Attitude Determination and Control*, chapter 17.1, pages 564–566. Kluwer Academic Publishers, 1978.

[15] Doug Wiemer. Private Correspondence, Aug. 2003.

[16] Doug Wiemer and Martha Houchens. "ACS Performance Modeling". PowerPoint presentation, Ball Aerospace and Technologies Corp., 2003.

[17] Darrell Zimbleman. Private correspondence, "Gyro Error Model for EOS AQUA", Sept. 2003.

[18] Darrell Zimbleman. "Modeling Gyro Noise". Technical report, NASA/Goddard Space Flight Center, 2003.